Reviews in Mineralogy & Geochemistry
Vol. 55, pp. 359-408, 2004

Isotopic Constraints on Biogeochemical Cycling of Fe

Clark M. Johnson and Brian L. Beard
Department of Geology and Geophysics
University of Wisconsin
Madison, Wisconsin, 53706, U.S.A.

Eric E. Roden
Department of Biological Sciences
University of Alabama
Tuscaloosa, Alabama, 35487, U.S.A.

Dianne K. Newman
Division of Geological and Planetary Sciences
California Institute of Technology
Pasadena, California, 91125, U.S.A.

Kenneth H. Nealson
Department of Earth Sciences
University of Southern California
Los Angeles, California, 90089, U.S.A.

INTRODUCTION

Cycling of redox-sensitive elements such as Fe is affected by not only ambient Eh-pH conditions, but also by a significant biomass that may derive energy through changes in redox state (e.g., Nealson 1983; Lovely et al. 1987; Myers and Nealson 1988; Ghiorse 1989). The evidence now seems overwhelming that biological processing of redox-sensitive metals is likely to be the rule in surface- and near-surface environments, rather than the exception. The Fe redox cycle of the Earth fundamentally begins with tectonic processes, where "juvenile" crust (high-temperature metamorphic and igneous rocks) that contains Fe which is largely in the divalent state is continuously exposed on the surface. If the surface is oxidizing, which is likely for the Earth over at least the last two billion years (e.g., Holland 1984), exposure of large quantities of Fe(II) at the surface represents a tremendous redox disequilibrium. Oxidation of Fe(II) early in Earth's history may have occurred through increases in ambient O_2 contents through photosynthesis (e.g., Cloud 1965, 1968), UV-photo oxidation (e.g., Braterman and Cairns-Smith 1987), or anaerobic photosynthetic Fe(II) oxidation (e.g., Hartman 1984; Widdel et al. 1993; Ehrenreich and Widdel 1994). Iron oxides produced by oxidation of Fe(II) represent an important sink for Fe released by terrestrial weathering processes, which will generally be quite reactive. In turn, dissimilatory microbial reduction of ferric oxides, coupled to oxidation of organic carbon and/or H_2, is an important process by which Fe(III) is reduced in both modern and ancient sedimentary environments (Lovley 1991; Nealson and Saffarini 1994). Recent microbiological evidence (Vargas et al.

1529-6466/04/0055-010B$05.00

1998), together with a wealth of geochemical information, suggests that microbial Fe(III) reduction may have been one of the earliest forms of respiration on Earth. It therefore seems inescapable that biological redox cycling of Fe has occurred for at least several billion years of Earth's history.

Significant Fe isotope variations in nature are generally restricted to relatively low-temperature systems, including hydrothermal fluids and chemically precipitated minerals (Beard and Johnson 1999; Beard et al. 1999; Zhu et al. 2000; Bullen et al. 2001; Sharma et al. 2001; Beard et al. 2003b; Johnson et al. 2003; Matthews et al. 2004). Experiments investigating metabolic processing of Fe have shown that measurable Fe isotope fractionations are produced during dissimilatory Fe(III) reduction by bacteria (Beard et al. 1999, 2003a; Icopini et al. 2004; Johnson et al. 2004a), as well as anaerobic photosynthetic Fe(II) oxidation (Croal et al. 2004). In addition, the role of organic ligands in promoting mineral dissolution has been investigated in experiments (Brantley et al. 2001, 2004). Iron isotopes may also be fractionated in abiologic systems, including ion-exchange chromatography (Anbar et al. 2000; Roe et al. 2003), abiotic precipitation of ferric oxides or oxyhydroxides (Bullen et al. 2001; Skulan et al. 2002), and sorption of aqueous Fe(II) to ferric hydroxides (Icopini et al. 2004). The largest abiotic fractionations in experiment have been measured between Fe(III) and Fe(II) species in solution, and both kinetic (Matthews et al. 2001) and equilibrium (Johnson et al. 2002; Welch et al. 2003) fractionations have been observed.

In this chapter we review some of the major pathways of biological Fe metabolism, and discuss experimental studies that have investigated Fe isotope fractionations in several systems. We largely focus on the results from experiments because our goal is to understand Fe isotope fractionations at a mechanistic level. We find that experimental results reflect both kinetic and equilibrium effects, sometimes in the same experiment, making it important to scale laboratory results to the kinetic realm of natural environments. An important concept that we develop is consideration of the residence time of Fe in the various reservoirs involved in biological processing of Fe relative to the timescales of isotopic exchange; this, in addition to evaluating the isotopic mass balance in a system, form the underpinnings for understanding the measured Fe isotope fractionations in experimental studies. We compare Fe isotope fractionations that are produced in abiologic and biologic systems, looking to situations where isotopic variations produced by biochemical cycling of Fe is likely to be found in nature. Throughout the chapter, we highlight some areas of future research that are critical to our understanding of Fe isotope geochemistry and its uses in tracing biogeochemical cycling of Fe.

Nomenclature

We discuss Fe isotope variations using standard δ notation, in units of per mil (parts per 1000, or ‰):

$$\delta^{56}\mathrm{Fe} = \left(\frac{{}^{56}\mathrm{Fe}/{}^{54}\mathrm{Fe}_{\mathrm{SAMPLE}}}{{}^{56}\mathrm{Fe}/{}^{54}\mathrm{Fe}_{\mathrm{BULK\ EARTH}}} - 1 \right) 10^3 \qquad (1)$$

where $^{56}Fe/^{54}Fe_{BULK\ EARTH}$ is defined by a wide variety of terrestrial and lunar igneous rocks that have $\delta^{56}Fe = 0.00 \pm 0.05$‰ (Beard et al. 2003a). Data from different laboratories may be compared using the IRMM-14 standard, which on the Bulk Earth scale defined above, has a $\delta^{56}Fe$ value of −0.09‰ (Beard et al. 2003a). Other notations are used in the literature, and the reader is referred to the previous chapter for a detailed discussion (Chapter 10A, Beard and Johnson 2004). When describing Fe isotope fractionations between coexisting phases A and B, we follow the traditional definitions for the isotope fractionation factor $\alpha_{A\text{-}B}$, which, in the case of Fe, is defined as:

$$\alpha_{A\text{-}B} = \frac{\left(^{56}Fe/^{54}Fe\right)_A}{\left(^{56}Fe/^{54}Fe\right)_B} \quad (2)$$

Note that $\alpha_{A\text{-}B}$ may reflect either kinetic or equilibrium isotope partitioning between phases A and B. As discussed in the previous chapter, $\alpha_{A\text{-}B}$ for $^{56}Fe/^{54}Fe$ ratios typically varies between 0.997 and 1.003 (Chapter 10A; Beard and Johnson 2004). In general, we will describe isotopic fractionations using $\Delta_{A\text{-}B}$, following standard definitions:

$$\Delta_{A\text{-}B} = \delta^{56}Fe_A - \delta^{56}Fe_B \approx 10^3 \ln \alpha_{A\text{-}B} \quad (3)$$

Given the range in Fe isotope compositions measured so far, use of the approximation $\Delta_{A\text{-}B}$ to describe isotopic fractionations introduces an error of at most 0.02‰, which is not significant relative to analytical uncertainties.

BIOLOGICAL PROCESSING OF IRON

Detailed understanding of the pathways by which biological processing of Fe occurs is required before we may identify the potential steps in which Fe isotope fractionation may be produced. Organisms process Fe in three general ways: (1) lithotrophic or phototrophic metabolism, where Fe(II) acts as an electron donor for energy generation and/or carbon fixation (e.g., Emerson 2000; Straub et al. 2001); (2) dissimilatory Fe(III) reduction, where Fe(III) acts as an electron acceptor for respiration (e.g., Nealson and Saffarini 1994); and (3) assimilatory Fe metabolism, which involves uptake and incorporation into biomolecules (e.g., Lowenstam 1981) (Table 1). For lithotrophic, phototrophic, and dissimilatory Fe metabolism, electron transfer occurs between the cell and Fe that is bound to the cell surface or incorporated in the outer membrane. Bacteria may cycle Fe through valence changes when it is energetically favorable for them to do so, and where they are able to out-compete abiotic redox reactions and other metabolic pathways that would naturally occur under specific conditions. For example, photosynthetic Fe(II) oxidation is generally restricted to anaerobic environments because high ambient O_2 contents would convert aqueous Fe(II) to ferric oxides at a rate that is substantially faster than oxidation by bacteria.

Fe(II) oxidation

Aqueous Fe(II) is common in many subaerial and submarine hot springs, and mid-ocean ridge hydrothermal activity likely provided a large source of soluble and reactive Fe(II) to the ancient oceans (e.g., Ewers 1983; Bau et al. 1997; Sumner 1997). Terrestrial weathering in the Archean, if it occurred under conditions of low atmospheric O_2 (e.g., Holland 1984), would have provided additional sources of soluble Fe(II). Photosynthesis, which may or may not involve a direct role for Fe, is likely to have been a major process for oxidizing Fe(II) over Earth's history. Molecular evidence suggests that anoxygenic photosynthesis evolved quite early in Earth's history (e.g., Xiong et al. 2000), although finding definitive morphologic or isotopic biomarkers in the rock record that would indicate the existence of photosynthesis or cycling of elements by bacteria in the Hadean or Early Archean has been challenging (e.g., Schopf 1993; Mojzsis et al. 1996; Eiler et al. 1997; Brasier et al. 2002; Fedo and Whitehouse 2002; Schopf et al. 2002).

Modern layered microbial communities provide a view into biochemical redox cycling. Oxidation of Fe(II) through high O_2 contents generated by cyanobacteria generally occurs in the top most (photic) portions of microbial mats. The upper, near-surface layers of microbial mats that are rich in cyanobacteria are commonly underlain by purple and green anoxygenic photosynthetic bacteria that thrive in the IR photic spectra (Stahl et al. 1985; Nicholson

Table 1. Biogeochemical cycles for Fe.

Metabolic pathways/organisms	*Electron donor/ acceptor*	*Oxygen levels*	*Product*
Fe(II) oxidation			
Photosynthesis			
Cyanobacteria	H_2O (donor)	oxygenic	Ferric oxide and hydroxide precipitation due to high ambient O_2.
Phototrophic Fe(II) oxidation			
"Purple bacteria" (e.g., *Rhodomicrobium*) "Green bacteria" (e.g., *Chlorobium*)	Fe(II) (donor)	anaerobic	Ferric oxide and hydroxide precipitation under anoxic conditions.
Chemolithotrophs			
Acidophiles (e.g., *Thiobacillus*)		oxygenic (low pH)	Ferric oxide and hydroxide precipitation.
Neutrophiles (e.g. *Gallionella*, ES1/ES2/PV1, TW2)		oxygenic (neutral pH)	Aqueous Fe(III).
Nitrate reduction	NO_3^- (acceptor)	anaerobic (in dark)	Aqueous Fe(III); Ferric oxide and hydroxide precipitation.
Dissimilatory Fe(III) reduction			
Shewanella; Geobacter; many others	Fe(III) (acceptor)		Aqueous Fe(II), $FeCO_3$, $CaFe(CO_3)_2$, Fe_3O_4, FeOOH.
Assimilatory Fe metabolism			Fe biomolecules (siderophores, ferritin); magnetite (magnetotactic bacteria).

et al. 1987); if atmospheric O_2 contents were low early in Earth's history, anoxygenic photosynthetic bacteria likely thrived on the surface of layered microbial communities. Although ferric oxide precipitates formed by cyanobacterial activity would not be directly related to metabolic processing of Fe, anoxygenic photosynthetic bacteria would derive energy from Fe(II) oxidation. It is expected that geochemical cycling of Fe in the upper layers of layered microbial communities will be dominated by Fe(II) oxidation, both in the presence and absence of oxygen, where Fe(II) may be supplied by the sediment substrate through dissolution of silicates, carbonates, or sulfides. In the case of mats associated with thermal springs, or in shallow marine settings, dissolved Fe(II) may be supplied by thermal or upwelling marine waters. The magnitude of visible radiation, oxygen gradients, and iron supply would be among some of the factors that govern the rate of ferric oxide deposition in

layered microbial communities (e.g., Pierson et al. 1999; Pierson and Parenteau 2000). The primary products of Fe(II) oxidation are ferric oxides or oxyhydroxides, and this process may provide a source of oxidants that may be exploited by anaerobic Fe(III)-reducing bacteria.

The importance of anaerobic photosynthetic Fe(II)-oxidation by bacteria was highlighted by Widdel et al. (1993), and these organisms may have played a major role in formation of ferric iron deposits in the absence of an oxygenated atmosphere. Experimental studies have used a variety of Fe(II) species as the electron donor, including $FeCO_3$, FeS, and $FeSO_4$, suggesting that these organisms may utilize a wide variety of Fe(II) sources. Some purple (non-sulfur) bacteria, such as *Rhodomicrobium vannielli*, become encased in ferric oxides, which ultimately limits their growth, and this has been taken as evidence that Fe(II) oxidation is a "side activity" in some cases (Heising and Schink 1998). In contrast, Fe(II)-oxidizing green bacteria such as *Chlorobium ferrooxidans* appear to precipitate ferric oxides that fall away from the cell and form ferric oxide deposits outside the cell region (Heising et al. 1999). Some Fe(III) may remain in solution, possibly bound by "iron solubilizing compounds" that are postulated to be excreted by the cells (Straub et al. 2001), although this hypothesis has not been confirmed in recent experimental studies (Kappler and Newman 2004).

Several other pathways for bacterially-related Fe(II) oxidation exist. In both circumneutral and low-pH hydrothermal systems, chemolithotrophic iron-oxidizing microorganisms may thrive under aerobic conditions (e.g., Emerson 2000; Ehrlich 1996). In addition, Fe(II)-oxidizing metabolism that involves NO_3^- as the terminal electron acceptor may occur in the absence of light (e.g., Straub et al. 2001). Nitrate-reducing bacteria may grow with or without Fe(II) as the electron donor where other compounds such as acetate may supply electrons (e.g., Straub et al. 1996). Although it is possible that anaerobic nitrate-reducing bacteria may have been a globally important means by which Fe(II) oxidation occurred in dark conditions in the absence of photosynthesis (e.g., Benz et al. 1998; Straub et al. 1996, 2001), it is not clear where the abundant nitrate needed for this process would come from.

Fe(III) reduction

Dissimilatory reduction of ferric oxide/hydroxide minerals such as hematite, goethite, and ferrihydrite occurs by a number of pathways (e.g., Lovley 1987; Nealson and Myers 1990). The occurrence of reductase components such as *c*-type cytochromes or proteins in the outer cell membranes (e.g., Gaspard et al. 1998; Magnuson et al. 2000; Myers and Myers 1993, 2000; Beliaev et al. 2001; DiCristina et al. 2002), although debated for some species (Seeliger et al. 1998; Lloyd et al. 1999), has been taken as evidence that direct contact between microorganisms and ferric oxide substrates is required for Fe(III) reduction. Experiments in which ferric substrates were physically isolated from the cells support the apparent requirement of direct contact for the strict anaerobes *Geobacter sulfurreducens* and *Geobacter metallireducens* (e.g., Lloyd et al. 1999; Nevin and Lovley 2000, 2002a,b). A number of workers, however, have proposed that Fe(III) may be solubilized prior to reduction (by Fe(III) chelating compounds) or reduced by redox-active electron shuttle compounds such as excreted quinones, phenazines, or natural humic substances (e.g., Lovley et al. 1996; Newman and Kolter 2000; Hernandez and Newman 2001; Shyu et al. 2002; Hernandez et al. 2004), raising the possibility that direct contact between microorganism and ferric iron substrate may not be required in all cases. Although the energy required to secrete large quantities of chelators or electron shuttle compounds may be an issue, many natural groundwater systems that are rich in organic carbon are also rich in humic substances that may act as shuttle compounds (e.g., Nevin and Lovley 2002b). Experiments in which the ferric substrate was physically isolated from the cells (Nevin and Lovley 2002a,b), as well as those which used adhesion-deficient strains of *Shewanella algae*, where physical attachment of cells to ferric iron substrate was significantly reduced as compared to other strains (Caccavo et al. 1997; Caccavo and Das 2002), have shown that ferric oxyhydroxide may be reduced

by some species of bacteria without physical contact. Using genetics to knock out flagellar biosynthesis, Dubiel et al. (2002) also showed that attachment does not appreciably affect Fe(III)-reduction rates. Although ferric oxyhydroxides have been found inside the cell, it remains unclear how common this may be and what role such intracellular minerals may play in dissimilatory Fe(III) reduction (Glasauer et al. 2002).

In addition to production of aqueous Fe(II) under anaerobic conditions, the end-products of dissimilatory Fe(III)-reduction may include Fe carbonates (siderite and ankerite) and magnetite (e.g., Lovley et al 1987; Roden and Zachara 1996; Fredrickson et al. 1998; Roden et al. 2002; Zachara et al. 2002). Goethite and lepidocrocite may also be produced where aqueous Fe(II) catalyzes phase transformation of poorly crystalline ferric hydroxides such as ferrihydrite (Hansel et al. 2003; Glasauer et al. 2003). Banded iron formations (BIFs) have been proposed as repositories for magnetite and Fe carbonate that may have formed through dissimilatory Fe(III) reduction (Nealson and Myers 1990). In addition, magnetite produced by magnetotactic bacteria has been proposed to occur in rocks spanning ages from the Proterozoic (Gunflint Formation) to modern sediments (e.g., Frankel et al. 1979, 1981; Chang and Kirschvink 1985; Chang et al. 1989). The rate of magnetite production on a per cell basis by dissimilatory Fe(III)-reducing bacteria is ~5,000 times greater than that at which magnetotactic bacteria produce magnetite (Konhauser 1998). Nevertheless, despite the vastly more rapid rate of magnetite production by dissimilatory Fe(III)-reducing bacteria, with a few notable exceptions (Karlin et. al. 1987; Eggar-Gibbs et al. 1999), production of magnetite by these organisms is relatively rare in modern environments.

Iron carbonate is a common early diagenetic phase in sedimentary rocks and occurs as either disseminated fine-grained authigenic material in sandstones and mud-rocks or as large (cm-sized or greater) concretions in mudrocks (Mozley 1989; Mozley and Wersin 1992; Mozley and Burns 1993; Macquaker et al. 1997; Uysal et al. 2000; Raiswell and Fisher 2000). In general, Fe carbonate is formed in anoxic diagenetic environments where the rate of Fe(III) reduction is greater than that of bacterial sulfate reduction (Pye et al. 1990; Coleman 1993). The growth of siderite apparently requires biotic mediation to provide the source of both Fe(II) and carbonate through oxidation of organic carbon coupled to dissimilatory Fe(III) reduction (Coleman 1993; Coleman et al. 1993). Authigenic Fe carbonates typically have much higher Mg and Ca contents than can be accommodated if they formed in thermodynamic equilibrium at low temperatures (e.g., Pearson 1974; Curtis et al. 1986; Mozley and Carothers 1992; Laverne 1993; Baker et al. 1995; Hendry 2002). These metastable compositions are significantly different as compared to Fe(II)-carbonates in, for example, BIFs, which tend to have compositions that are similar to those expected for formation under equilibrium conditions (Machamer 1968; Butler 1969; Floran and Papike 1975; Klein 1974, 1978; Lesher 1978; Klein and Gole 1981; Klein and Beukes 1989; Beukes and Klein 1990). The apparently non-equilibrium major-element compositions of many authigenic carbonates suggests that such compositions may identify biologically-mediated carbonate precipitation, and may represent a "biomarker" in and of themselves.

Implications for Fe isotope fractionations

Phase transformations that occur through biological processing of Fe may produce isotopic fractionations that are distinct from those in "equivalent" abiologic systems if organic ligands produce distinct isotopic effects, or if biology produces kinetic or equilibrium conditions or Fe products that are not commonly found in abiologic systems. For example, of the four pathways for Fe(II) oxidation illustrated in Figure 1, those which involve Fe(II) as the electron donor (e.g., anoxic photosynthetic Fe(II) oxidation) are most likely to be intimately bound to the cell so that electron transfer is facilitated, raising the possibility that Fe isotope fractionations produced by these pathways may be distinct from those where oxidation occurs indirectly, such as through oxygenic photosynthesis. The large number of different pathways and related reactions

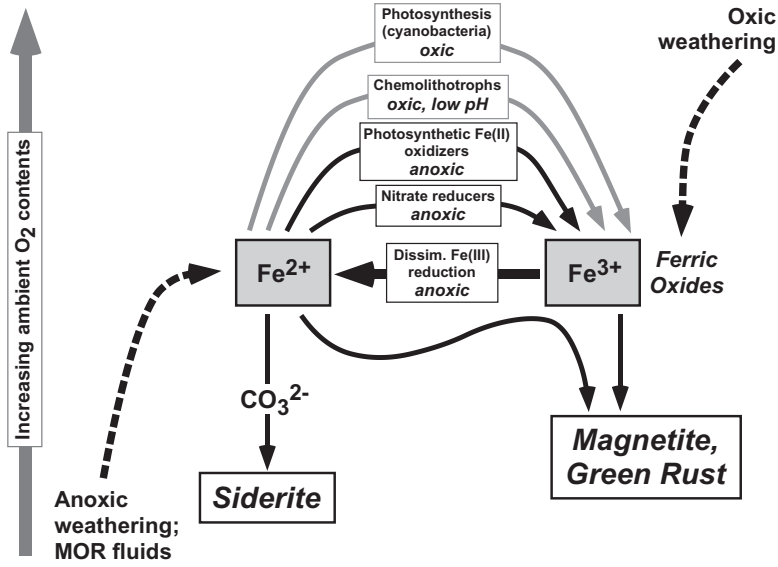

Figure 1. Schematic diagram of Fe redox cycling through biological processes. A large number of pathways are involved in dissimilatory Fe(III) reduction, as listed in Table 2. Processes that occur under oxic conditions are placed near the upper part of the diagram, and those that occur under anoxic conditions are placed in the lower part of the diagram. Major lithologic sources of Fe are noted for high and low oxygen environments.

involved in reduction of ferric hydroxides listed in Table 2 highlights the many opportunities to produce Fe isotope fractionations among the various reduction products, including aqueous Fe(II), sorbed Fe, and a wide variety of solid products. If some of these components are isotopically distinct and unlikely to be present in the absence of biology, it is possible to produce isotopic variations that may be confidently ascribed to biochemical cycling. Finally, the diverse pathways involved in Fe biochemical cycling may record distinct fractionations under equilibrium and kinetic conditions, requiring consideration of the rates of biochemical processing of Fe in laboratory experiments as compared to those expected in nature.

ISOTOPIC FRACTIONATION DURING DISSOLUTION AND PRECIPITATION OF MINERALS

Dissolution of minerals, such as may occur during dissimilatory Fe(III) reduction, or precipitation of new biominerals during reductive or oxidative processing of Fe, represent important steps in which Fe isotope fractionation may occur. We briefly review several experiments that have investigated the isotopic effects during mineral dissolution, as well as calculated and measured isotopic fractionations among aqueous Fe species and in fluid-mineral systems. In some studies, the speciation of aqueous Fe is unknown, and we will simply denote such cases as $Fe(III)_{aq}$ or $Fe(II)_{aq}$.

Congruent dissolution

The term "congruent dissolution" often refers to a process by which a mineral is dissolved in stoichiometric proportions into solution without formation of a new solid phase, and this usage is convenient for isotopic studies because it constrains the phases or components that may

Table 2. Biogenic Fe(III) reduction pathways.

Process	*Example Reactions*
HFO reductive dissolution[1]	$8Fe(OH)_3(s) + CH_3COO^- + 15H^+ = 8Fe^{2+} + 2HCO_3^- + 20H_2O$ (acetate oxidation)
	$4Fe(OH)_3(s) + CH_3CHOHCOO^- + 7H^+ = 4Fe^{2+} + CH_3COO^- + HCO_3^- + 10H_2O$ (lactate oxidation)
Ferric hydroxide phase conversion[2]	$Fe(OH)_3 + Fe^{2+} = \alpha\text{-}FeO{\cdot}OH + H_2O + Fe^{2+}$
	$Fe(OH)_3 + Fe^{2+} = \gamma\text{-}FeO{\cdot}OH + H_2O + Fe^{2+}$
Fe carbonate precipitation[3]	$Fe^{2+} + HCO_3^- = FeCO_3(s) + H^+$
	$Ca^{2+} + Fe^{2+} + 2HCO_3^- = CaFe(CO_3)_2(s) + 2H^+$
Ferrous hydroxide precipitation[4]	$Fe^{2+} + 2H_2O = Fe(OH)_2(s) + 2H^+$
Magnetite formation[5]	$2Fe(OH)_3 + Fe^{2+} = Fe_3O_4 + 2H_2O + 2H^+$
Mixed Fe(II)-Fe(III) hydroxide ("green rust") formation[6]	$2Fe(OH)_3 + 4Fe^{2+} + A^{2-}(OH^-, CO_3^{2-}, SO_4^{2-}, Cl^-) + 9H_2O = [Fe^{II}_4Fe^{III}_2(OH)_{12}][A^{2-}{\bullet}3H_2O] + 6H^+$
Fe(II) surface complexation (to HFO, magnetite, or "green rust" surfaces)[7]	$\equiv Fe^{III}OH + Fe^{2+} + H_2O = \equiv Fe^{III}OFe^{II}OH_2^+ + H^+$
$Fe(OH)_2$ surface precipitation (on HFO, magnetite, or "green rust" surfaces)[8]	$\equiv Fe^{III}OH + nFe^{2+} + (2n-1)H_2O = \equiv Fe^{III}O(Fe(OH)_{2(s)})_{n-1}{=}FeOH_2^+ + (2n-1)H^+$

Reduction pathways listed are those that occur for HFO as the terminal electron acceptor.

References:

[1] Fredrickson et al. (1998); Lovley and Phillips (1988).
[2] Zachara et al. (2002); Glasauer et al. (2003); Hansel et al. (2003).
[3] Fredrickson et al. (1998); Lovley and Phillips (1988); Postma (1977; 1981; 1982); Roden and Lovley (1993); Roden et al. (2002); Zachara et al. (2002).
[4] Mandal (1961).
[5] Ardizzone and Formaro (1983); Lovley et al. (1987); Lovley and Phillips (1988); Mann et al. (1989); Roden and Lovley (1993); Fredrickson et al. (1998); Zachara et al. (2002).
[6] Fredrickson et al. (1998); Roden et al. (2002); Zachara et al. (2002).
[7] Farley et al. (1985); Dzombak and Morel (1990); Fredrickson et al. (1998); Appelo et al. (2002); Roden and Urrutia (2002).
[8] Farley et al. (1985); Dzombak and Morel (1990); Haderlein and Pecher (1999); Roden and Urrutia (2002).

develop isotopically distinct compositions. Congruent dissolution may occur through complex interactions with heterogeneous surfaces and boundary layers (e.g., Jeschke and Dreybrodt 2002), but may be satisfactorily described as a progressive stripping of layers or sections from the mineral surface. If the mineral is isotopically homogeneous, no isotopic contrast should exist between solid and dissolved components. Although preferential extraction of one isotope might be envisioned to occur within surface monolayers or other surface sections, such a process would create an excess of the excluded isotope as successive surface sections are removed, balancing the overall isotope composition of the dissolved material to be equal to that of the bulk solid. Partial dissolution of μm- to 100 nm-size hematite crystals in HCl confirms that no measurable Fe isotope fractionation occurs during congruent partial dissolution (Fig. 2). The low pH of these experiments ensured that $Fe(III)_{aq}$ does not precipitate and form an additional phase that might have a different isotopic composition than Fe in solution. In the experiments illustrated in Figure 2, partial dissolution of hematite in HCl likely dissolves complete surface sections of hematite crystals, and is distinct from a leaching process that selectively removes a specific element from a portion of the crystal in non-stoichiometric proportions; the later process would be considered incongruent dissolution, and for the purposes of characterizing isotopically distinct reservoirs, this may be considered a new phase. In addition to the studies of hematite dissolution, Brantley et al. (2004) investigated abiotic dissolution of goethite in the presence of the siderophore desferrioxamine mesylate (DFAM), and found that dissolution occurred congruently, where the isotopic composition of Fe in solution was identical to that of the ferric hydroxide starting material.

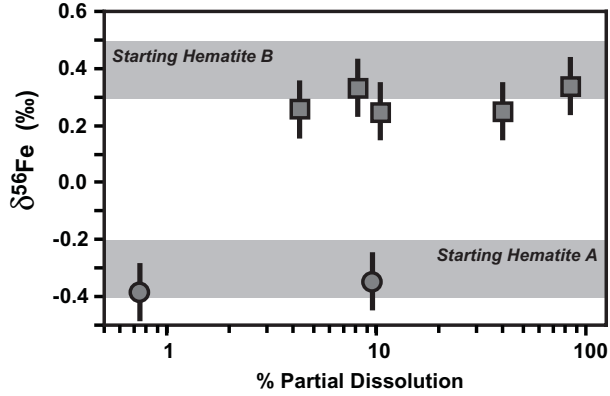

Figure 2. Isotopic effects of congruent partial dissolution of hematite. Within the 2σ error of the analyses, there is no significant Fe isotope fractionation over wide ranges of percent dissolution. Gray bars denote bulk composition (2σ) of the two hematite grains. Data from Skulan et al. (2002) and Beard et al. (2003a).

Incongruent dissolution

Significant Fe isotope fractionations may be produced during incongruent dissolution in the presence of organic ligands (Brantley et al. 2001, 2004). Dissolution of hornblende by siderophore-producing bacteria was shown to be enhanced relative to abiologic dissolution, and was interpreted to reflect preferential extraction of Fe from the mineral, accompanied by creation of an Fe-depleted layer in at least the upper 100 Å of the mineral surface (Kalinowski et al. 2000; Liermann et al. 2000). Because preferential mobilization of elements occurred, as shown by changing Fe/Si and Fe/Al ratios, the Fe-depleted layer represents a new phase. The extent of Fe leaching and apparent isotopic shift for aqueous Fe increased with increasing

ligand association constant for abiotic experiments, where the largest effects (~0.3‰) were observed for the siderophore DFAM (Fig. 3). Larger isotopic contrasts between aqueous Fe and the initial hornblende were observed for leaching in bacterial cultures, on the order of 0.5 to 0.8‰ (Fig. 3).

Brantley et al. (2001) interpret Fe isotope fractionation to occur during hydrolysis of surface complexes, and to reflect a kinetic isotope fractionation that is dependent upon the strength of the organic ligand. The isotopic fractionations measured in the experiments of Brantley et al. (2001) reflect those produced during very small extents of dissolution or leaching, where at least 0.037% dissolution/leaching occurred based on estimation of the Fe content of the hornblende and reported Si/Al and Fe/Si ratios. Assuming spherical grains of an average diameter of 340 μm (Brantley et al. 2001), the minimum thickness of the leached layer may be calculated at ~210 Å. Based on isotopic mass-balance, the δ^{56}Fe value of the Fe-depleted layer would be relatively high, where the highest values would be associated with a relatively thin leached layer, and rapidly decrease if the thickness of the leach layer was greater. If the leached layer was 250 Å thick, its δ^{56}Fe value, based on mass balance, should be almost 5‰ higher that that of the Fe in solution; at 500 Å thickness, the leached layer should be ~1.5‰ higher than Fe in solution.

In a more detailed study, Brantley et al. (2004) observed non-stoichiometric dissolution of hornblende in abiotic experiments using acetate, oxalate, citrate, and siderophore (DFAM), where the δ^{56}Fe values of the aqueous Fe that was released became more negative in this order, relative to the starting material. The isotopic fractionations were modeled as a kinetic process during transport of Fe through the surface leached layer. This model predicts that significant changes in the δ^{56}Fe value for aqueous Fe will occur before the system reaches steady-state conditions during dissolution.

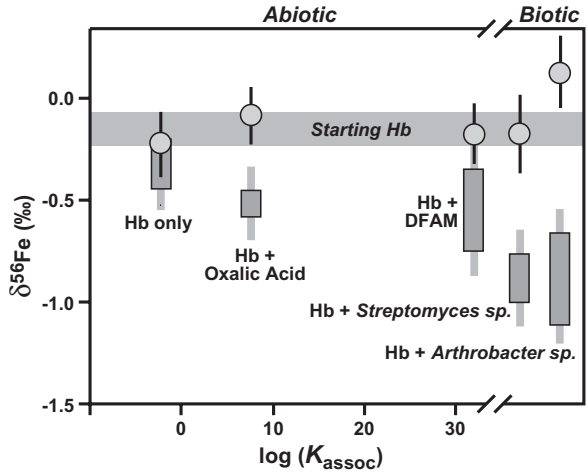

Figure 3. Effects on Fe isotope compositions of partial dissolution of hornblende in the presence of various organic ligands, as well as *Streptomyces* and *Arthrobacter* bacteria (identification of *Arthrobacter sp.* has been revised to *Bacillus sp.*; S. Brantley, pers. commun. 2004). For abiotic experiments, Fe isotope data are plotted relative to the association constant (K_{assoc}) for the indicated ligands. Fe isotope composition of starting hornblende shown in gray bar. Gray circles reflect Fe isotope composition of residual hornblende (error bars noted), and gray boxes denote range in δ^{56}Fe values measured for aqueous Fe (error bars shown) after partial dissolution. Partial dissolution occurs incongruently in these experiments, accompanied by formation of an Fe-poor leached layer in the hornblende. Data from Brantley et al. (2001).

The processes by which Fe isotope fractionations are associated with mineral dissolution and leaching by organic molecules, including those produced by bacteria, remains little explored, but, as Brantley et al. (2001, 2004) point out, are important components to understanding Fe isotope variations in natural weathering systems. At very small extents of dissolution or leaching (<0.1%; Brantley et al. 2001), it is difficult to constrain the reservoirs involved in producing isotopic fractionations because the Fe reservoirs that are complementary to the isotopically light aqueous Fe are difficult to identify, let alone analyze. Partial extractions of labile Fe components from soils show that these components may have δ^{56}Fe values that are significantly lower than the bulk solid, which is interpreted to reflect the effects of incongruent, non-stoichiometric dissolution of silicate minerals by Fe-organic complexes (Brantley et al. 2001, 2004). These results indicate that soils may contain isotopically variable components when soil formation involves organic substances that dissolve minerals incongruently. In terms of large-scale Fe cycling, it seems most likely that the isotopic variations of these labile components will be seen in the dissolved load of Fe in hydrologic systems; they are not apparently recorded in the bulk clastic detritus of eolian and fluvial systems, given the isotopic homogeneity of bulk clastic material (Beard et al. 2003b).

Isotopic fractionations among aqueous species and minerals in abiologic systems

Significant isotopic fractionations are observed among several Fe-bearing aqueous species and solid phases in abiologic systems that are pertinent to biochemical processing of Fe (Tables 1 and 2). Some of the largest Fe isotope fractionations occur between oxidized and reduced species (Polyakov and Mineev 2000; Schauble et al. 2001), where, for example, the experimentally determined equilibrium isotope fractionation between $[Fe^{III}(H_2O)_6]^{3+}$ and $[Fe^{II}(H_2O)_6]^{2+}$ ($\Delta_{Fe(III)aq-Fe(II)aq}$) at room temperature is +2.9‰ (Johnson et al. 2002; Welch et al. 2003). The equilibrium isotope fractionation between $[Fe^{III}(H_2O)_6]^{3+}$ and Fe_2O_3 (hematite) is estimated to be ~ −0.1‰ at room temperature (Skulan et al. 2002). Experimental determination of the equilibrium isotope fractionation between $[Fe^{II}(H_2O)_6]^{2+}$ and $FeCO_3$ (siderite) is estimated to be +0.5‰ at room temperature (Wiesli et al. 2004). It remains unknown if the large isotopic effects that are predicted for Ca, Mg, and Mn substitution into Fe carbonates (Polyakov and Mineev 2000), up to 1.5‰ at room temperature, will be confirmed by experimental studies in abiologic systems. Isotopic fractionation between $[Fe^{II}(H_2O)_6]^{2+}$ and Fe_3O_4 (magnetite) is predicted to be −4.2‰ at room temperature under equilibrium conditions, but this has yet to be confirmed experimentally; experimental confirmation of predicted fractionations is important, because in many cases the predicted Fe isotope fractionations based on theory have been shown to be significantly different from those determined by experiment. The reader is referred to the previous chapter (Chapter 10A; Beard and Johnson 2004) for a more detailed discussion of predicted and measured Fe isotope fractionation factors in abiologic systems. We will return to the fractionations in abiologic systems in later sections.

ISOTOPIC MASS BALANCE

In complex systems that involve multiple Fe-bearing species and phases, such as those that are typical of biologic systems (Tables 1 and 2), it is often difficult or impossible to identify and separate all components for isotopic analysis. Commonly only the initial starting materials and one or more products may be analyzed for practical reasons, and this approach may not provide isotope fractionation factors between intermediate components but only assess a net overall isotopic effect. In the discussions that follow on biologic reduction and oxidation, we will conclude that significant isotopic fractionations are likely to occur among intermediate components.

We illustrate some examples of the differences between apparent (measured) Fe isotope fractionations between starting materials and a single product and those that are postulated

to occur among intermediate products in Figure 4. In calculating the isotopic mass balance during mineral leaching (Brantley et al. 2001), a leached layer thickness of 500 Å is assumed in calculating the δ^{56}Fe value for the leach layer, which results in a calculated fractionation between the leached layer and $Fe(II)_{aq}$ of +1.5‰ (Fig. 4). The correlation of increasing percent leaching with increasing ligand association constant (K_{assoc}) observed by Brantley et al. (2001, 2004) indicates that the isotopic mass balance between the leached layer and aqueous Fe was likely to have changed. Brantley et al. (2004) interpret their data to reflect kinetic fractionation during transport through a leached layer. It is, however, possible that the observed correlation between δ^{56}Fe values for $Fe(II)_{aq}$ and K_{assoc} (Fig. 3) in part reflects changes in the isotopic mass balance of the leached layer and aqueous Fe rather than a kinetic isotope fractionation that is dependent upon K_{assoc}, and demonstrates the importance of assessing isotopic mass balance in experiments.

In the sorption experiments of Icopini et al. (2004), the measured isotopic contrast between $Fe(II)_{aq}$ and the goethite starting material was −0.8‰ after Fe(II) had sorbed to the surface over 24 hours; in this case, the isotopic fractionation between sorbed Fe(II) and $Fe(II)_{aq}$ is not the 0.8‰ *measured* difference, but is approximately +2.1‰ based on an inferred δ^{56}Fe value for the sorbed component as calculated from Fe mass balance (Fig. 4), as was noted in that study. Measured differences in Fe isotope compositions between ferric oxide/hydroxide and $Fe(II)_{aq}$ during dissimilatory Fe(III) reduction and photosynthetic Fe(II) oxidation have been proposed to reflect fractionation between soluble Fe(II) and Fe(III) species, where the soluble Fe(III) component is postulated to be bound to the cell and is not directly measured (Beard et al. 2003a; Croal et al. 2004). In the case of dissimilatory Fe(III) reduction, assuming a static model simply for purposes of illustration, if 50% of the Fe in a pool that is open to

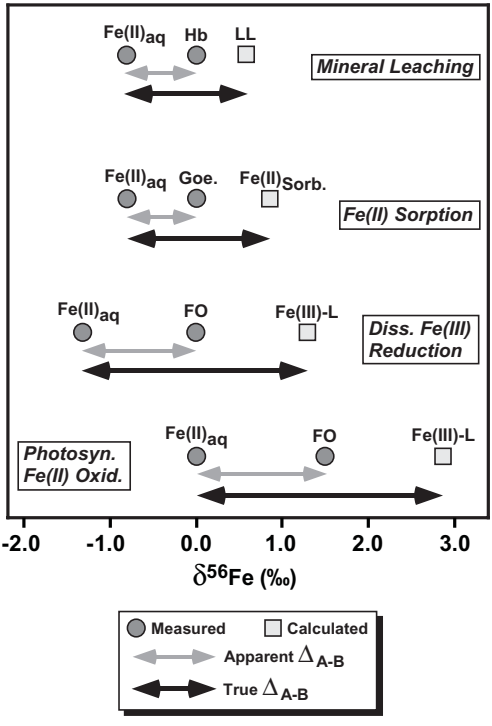

Figure 4. Examples of Fe isotope mass balance in experimental systems that have studied Fe isotope fractionation in biological systems or those that are pertinent to biogeochemical processing of Fe. Dark gray circles reflect measured Fe isotope compositions (where one component has been normalized to δ^{56}Fe=0.0) Light gray squares reflect calculated or inferred Fe isotope compositions for a component that is inferred from isotopic mass balance in the experiments, but which has not been analyzed directly. Data for mineral leaching from Brantley et al. (2001), and inferred δ^{56}Fe value for leached Fe layer ("LL") based on calculations described in the text. Data for Fe(II) sorption to goethite ("Goe.") from Icopini et al. (2004), and inferred δ^{56}Fe value for sorbed Fe based on calculations presented in that study. δ^{56}Fe value for ligand-bound Fe(III) ("Fe(III)-L") based on discussion of dissimilatory Fe(III) reduction of ferric oxide/hydroxide ("FO") in Beard et al. (2003a) and in the text, assuming a 50:50 mixture of $Fe(II)_{aq}$ and Fe(III)-L. δ^{56}Fe values for anaerobic photosynthetic Fe(II) oxidation based on inferred soluble Fe(III) component ("Fe(III)-L") as discussed in text and in Croal et al. (2004).

isotopic exchange occurs as ligand-bound Fe(III) (not measured) and the remaining 50% exists as $Fe(II)_{aq}$ (measured), then the 1.3‰ *measured* differences in isotopic compositions between the ferric oxide/hydroxide starting material and $Fe(II)_{aq}$ may actually reflect a +2.6‰ fractionation between the intermediate species of ligand-bound Fe(III) and the final $Fe(II)_{aq}$ product (Fig. 4). Similarly, the differences in isotopic compositions between $Fe(II)_{aq}$ starting material and ferric hydroxide precipitate formed during anaerobic photosynthetic Fe(II) oxidation may in fact reflect the combined effect of a large fractionation between ligand-bound Fe(III) and $Fe(II)_{aq}$, followed by a second fractionation between Fe(III) and the ferric hydroxide precipitate (Croal et al. 2004); the $\delta^{56}Fe$ value of the ligand-bound Fe(III) in such a model would be quite high (Fig. 4).

ISOTOPIC FRACTIONATION PRODUCED DURING DISSIMILATORY Fe(III) REDUCTION

Of the variety of ways in which Fe may be biologically processed (Table 1; Fig. 1), experimental investigation of dissimilatory Fe(III) reduction, which we will hereafter refer to as DIR, has received by far the most attention. Experimental studies of DIR have highlighted the importance of intermediate phases or species such as Fe(III) and Fe(II) surface complexes or poorly-crystalline solids (Table 2) to producing a range of end products. Ferrihydrite has been most commonly used as the terminal electron acceptor, which is often referred to as hydrous ferric oxide (HFO) in the biological literature, and we will follow this convention. More crystalline sources of electron acceptors such as hematite (Fe_2O_3), goethite (α-FeOOH), or lepidocrosite (γ-FeOOH) have been used as well. Reduction of Fe(III)-bearing clay minerals such as smectite is now recognized as an important component to DIR in natural systems (e.g., Kostka et al. 1996, 2002; Kim et al. 2004). Production of magnetite and Fe carbonates is readily identifiable in XRD spectra, but several non-aqueous, Fe(II)-bearing components that may be produced during DIR are more difficult to identify. Production of $Fe(OH)_2(s)$ has been identified, as well as mixed Fe(II)-Fe(III) hydroxide, or "green rust" (Table 2), which may also contain carbonate ion in high-carbonate systems. Surface complexation or sorption of Fe(II) on oxide minerals, either ferric oxide/hydroxide starting materials or a product such as magnetite may represent a significant repository of labile Fe(II) during DIR (Table 2). Fredrickson et al. (1998) demonstrated that intermediate Fe(II) and Fe(III) phases may be identified through extraction from partially reacted HFO or reduced products in 0.5 M HCl, followed by careful assays of Fe(III) and Fe(II) contents.

A key component to understanding Fe isotope fractionations produced by DIR seems likely to be the fate of Fe(III) following dissolution of the ferric oxide/hydroxide starting material, given the large isotopic fractionations that occur between oxidized and reduced phases (Polyakov and Mineev 2000; Schauble et al. 2001; Johnson et al. 2002; Welch et al. 2003; Anbar et al. 2004). Experiments in which the ferric substrate was isolated from contact with bacterial cells using *Geothrix fermentans* (a strict anaerobe) or *Shewanella algae* (a facultative anaerobe) did not prevent Fe(III) reduction (Nevin and Lovley 2002a,b), and significant quantities of soluble Fe(III) were measured in these experiments. In both the *G. fermentans* and *S. algae* experiments, ~10% of the soluble Fe in solution existed as $Fe(III)_{aq}$ over the course of the 15–20 day experiments. The $Fe(III)_{aq}/Fe(II)_{aq}$ ratio was relatively constant over time, including time periods when total aqueous Fe was increasing, as well as decreasing at later time periods when precipitation of Fe(II)-bearing phases may have occurred (Nevin and Lovley 2002a,b). The significant quantity of $Fe(III)_{aq}$ in these experiments stands in contrast to parallel experiments using *Geobacter metallireducens*, which did not produce measurable quantities of $Fe(III)_{aq}$ when *G. metallireducens* was isolated from physical contact with the ferric substrate (Nevin and Lovley 2002b). It has been hypothesized that the $Fe(III)_{aq}$ produced in the *G. fermentans* and *S. algae* experiments reflects release of electron shuttling compounds

and/or Fe(III) chelators (Nevin and Lovley 2002a,b). In experiments using *S. algae* where the cells were allowed free contact with the ferric substrate, however, no detectable $Fe(III)_{aq}$ existed (Johnson et al. 2004a). Nevertheless, the evidence seems to support a model where Fe(III) is first solubilized by an organic ligand, followed by reduction and release to the ambient aqueous solution and/or reacted to form a solid phase, although the quantity of "soluble" Fe(III) may be quite variable depending upon the organism and experimental conditions.

The process of DIR may be conceptualized as a series of reactions that occur at various rates and produce changing pools of Fe that are able to undergo isotopic exchange to variable degrees. Isotopic fractionations generally occur through uni-directional processes such as precipitation, or through exchange between pools of an element that are open to isotopic exchange over the timescales of the process. Based in part on the evidence that at least some species of bacteria solubilize Fe(III) during DIR, Beard et al. (2003a) hypothesized that the −1.3‰ fractionation in $^{56}Fe/^{54}Fe$ ratios measured between $Fe(II)_{aq}$ and ferric oxide/hydroxide substrate (the electron acceptor) may primarily reflect isotopic fractionation between pools of ligand-bound Fe(III) and Fe(II) that are open to isotopic exchange (Fig. 5). For the moment, we will ignore the effects of other reduced products such as Fe carbonate and magnetite, as well as the effects of Fe(II) that may be sorbed to solid phases, although these issues will be discussed in detail later. The first stage in which Fe isotope fractionation may occur during DIR is upon dissolution (Δ_1, Fig. 5). If dissolution occurs congruently, however, no Fe isotope fractionation is expected, as discussed above. The second step in which isotopic fractionation may occur is during reduction (Δ_2, Fig. 5), between ligand-bound or ambient Fe(II) and soluble Fe(III) that is delivered to the cell via an electron shuttle or extracellular protein. It is also possible that isotopic fractionation may occur between ligand-bound Fe(III) and the ferric substrate (Δ_3, Fig. 5), although isotopic exchange with solids at low temperatures will be quite slow. Finally, isotopic fractionation may occur between $Fe(II)_{aq}$ and Fe(II) that is sorbed to the ferric substrate (Δ_4, Fig. 5).

When viewed in a temporal context, the model illustrated in Figure 5 implicitly predicts changes in the proportions of ferric substrate, ligand-bound Fe(III), and the Fe(II) product over

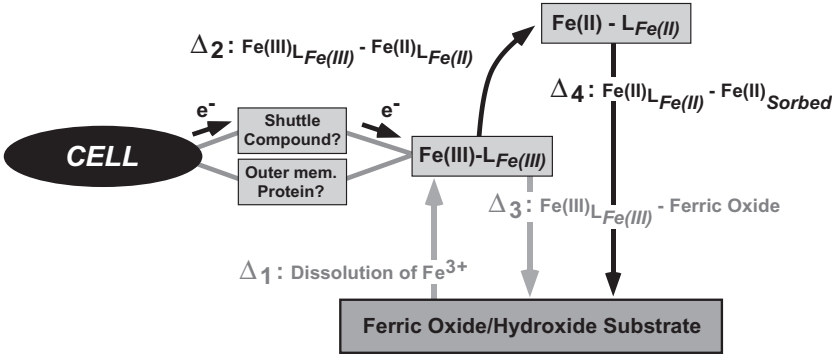

Figure 5. Possible pathways by which Fe isotopes may be fractionated during dissimilatory Fe(III) reduction (DIR). Dissolution, if it occurs congruently, is unlikely to produce isotopic fractionation (Δ_1). If Fe(II) is well complexed in solution and conditions are anaerobic, precipitation of new ferric oxides (Δ_3) is unlikely to occur. Significant isotopic fractionation is expected during the reduction step (Δ_2), possibly reflecting isotopic fractionation between soluble pools of Fe(III) and Fe(II). The soluble Fe(III) component is expected to interact with the cell through an electron shuttle compound and/or an outer membrane protein, and is not part of the ambient pool of aqueous Fe. Sorption of aqueous or soluble Fe(II) to the ferric oxide/hydroxide substrate (Δ_4) is another step in which isotopic fractionation may occur. Modified from Beard et al. (2003a).

time as reduction proceeds. For completeness, we hypothesize that two Fe(II) components exist, one bound to the cell immediately after reduction, and one that accumulates in the ambient pool of $Fe(II)_{aq}$. We therefore assume that the reduction process, where the initial ferric substrate is hematite (Fe_2O_3) or HFO/ferrihydrite (denoted as $Fe(OH)_3$ for simplicity), may be described as:

$$Fe_2O_3 \text{ or } Fe(OH)_3 \rightarrow Fe(III)\text{-}L_{Fe(III)} \rightarrow Fe(II)\text{-}L_{Fe(II)} \rightarrow Fe(II)_{aq} \quad (4)$$

where the ligand-bound Fe(III) is the terminal electron acceptor ("$Fe(III)\text{-}L_{Fe(III)}$"; Fig. 5), and Fe(II) is the immediate reduced product, possibly bound to organic ligands ("$Fe(II)\text{-}L_{Fe(II)}$"), and eventually released to a larger pool of Fe(II), including $Fe(II)_{aq}$. In terms of quantities that may be measured for their Fe isotope compositions, these would include the ferric substrate, $Fe(II)_{aq}$, and likely $Fe(II)\text{-}L_{Fe(II)}$ (although not a discrete phase) if this exists in the aqueous solution component. We assume that the $Fe(III)\text{-}L_{Fe(III)}$ component is *not* represented in a sample of the ambient aqueous solution, but instead is closely bound to or associated with the cells.

Fe(II) production during experiments investigating Fe isotope fractionation coupled to DIR generally followed a first-order rate law in terms of the rate of production of total Fe(II) (Beard et al. 1999, 2003a; Johnson et al. 2004a). Exponential regressions of the total Fe(II) contents (liquid + solid) versus time for these experiments produce high R^2 values (>0.95 for all but one case), and show that the initial reduction rates are a function of substrate, cell densities, and growth media, varying over a factor of 300 for these studies. The proportions of possible phases involved in DIR may be calculated using first-order kinetics, assuming a closed system and no initial product phases. The pertinent rate equations are:

$$\frac{d[Fe_2O_3]}{dt} = -k_1[Fe_2O_3] \quad (5)$$

$$\frac{d[Fe(III)\text{-}L_{Fe(III)}]}{dt} = k_1[Fe_2O_3] - k_2[Fe(III)\text{-}L_{Fe(III)}] \quad (6)$$

$$\frac{d[Fe(II)\text{-}L_{Fe(II)}]}{dt} = k_2[Fe(III)\text{-}L_{Fe(III)}] - k_3[Fe(II)\text{-}L_{Fe(II)}] \quad (7)$$

$$\frac{d[Fe(II)]}{dt} = k_3[Fe(II)\text{-}L_{Fe(II)}] \quad (8)$$

where we have represented the substrate as hematite and where k_1, k_2, and k_3 are first-order rate constants.

In this model, Fe isotope exchange is envisioned to most likely occur between "soluble" Fe(III) and Fe(II) components, such as $Fe(III)\text{-}L_{Fe(III)}$ and $Fe(II)\text{-}L_{Fe(II)}$ (Beard et al. 2003a), although only the $Fe(II)_{aq}$ component is measured. If this model is valid, a critical issue is whether isotopic equilibrium may be attained between these soluble pools of Fe, despite the changing reservoir sizes and fluxes that occur through Equations (5)–(8). As noted in the previous chapter (Chapter 10A; Beard and Johnson 2004), attainment of isotopic equilibrium will depend upon the elemental residence time in an Fe pool relative to the time required for isotopic exchange. We can define the residence time for Fe(III)-L, for example, using standard definitions, as:

$$\tau_{Fe(III)\text{-}L} = \frac{M_{Fe(III)\text{-}L}}{J_{Fe(III)\text{-}L}} \quad (9)$$

where $M_{Fe(III)\text{-}L}$ is the total moles of Fe in the Fe(III)-$L_{Fe(III)}$ reservoir, and $J_{Fe(III)\text{-}L}$ is the flux of Fe through the Fe(III)-$L_{Fe(III)}$ reservoir. Substituting the rate equations into Equation (9), we obtain:

$$\tau_{Fe(III)_{aq}} = \frac{\left[Fe(III)\text{-}L_{Fe(III)}\right]}{k_1\left[Fe_2O_3\right] - k_2\left[Fe(III)\text{-}L_{Fe(III)}\right]} \tag{10}$$

If we define the time to reach isotopic equilibrium through isotopic exchange as t_{ex}, then we can expect isotopic equilibrium to be attained between [Fe(III)-$L_{Fe(III)}$] and [Fe(II)-$L_{Fe(II)}$] when:

$$\tau_{Fe(III)\text{-}L} \gg t_{ex} \tag{11}$$

It is important to note that, as discussed in the previous chapter (Chapter 10A; Beard and Johnson 2004), attainment of isotopic equilibrium is not related to the time required to reach steady-state in terms of the concentration or molar ratios of Fe in various species, such as the [Fe_2O_3]/[Fe(III)-$L_{Fe(III)}$] ratio. The time required to reach isotopic equilibrium (t_{ex}) has been determined for Fe(III)-Fe(II) exchange in dilute aqueous solutions of varying Cl^- contents, and isotopic equilibrium is essentially complete within ~10 seconds at room temperature (Welch et al. 2003). It is possible that t_{ex} is significantly longer if Fe(III) and/or Fe(II) are bound to strong organic ligands, but it seems unlikely that t_{ex} could exceed timescales of hours; this inference, however, needs to be confirmed by experiments.

Assuming that $k_2 > k_1$ and $k_3 > k_1$, the system will eventually reach steady-state in terms of the concentration ratios of [Fe_2O_3]/[Fe(III)-$L_{Fe(III)}$] and [Fe_2O_3]/[Fe(II)-$L_{Fe(II)}$]. The time to reach steady-state in, for example, the [Fe_2O_3]/[Fe(III)-$L_{Fe(III)}$] ratio, may be defined as:

$$t_{\text{Steady State}} = 1/k_2 \tag{12}$$

(Lasaga 1981), although more conservative formulations tend to be used in the short-lived radionuclide literature that are related to the half-life, such as:

$$t_{\text{Steady State}} = n\left(\ln 2/k_2\right) \tag{13}$$

We will use Equation (13) to define the time to reach steady-state, setting $n = 7$ because this provides a close match to the time required to reach steady-state in Figure 6.

Calculation of Fe isotope compositions

Once temporal changes in the relative proportions of the species Fe_2O_3, Fe(III)-$L_{Fe(III)}$, Fe(II)-$L_{Fe(II)}$, and $Fe(II)_{aq}$ are computed, the $\delta^{56}Fe$ values for the various components may be defined by a simple mass-balance equation:

$$\delta_{Sys} = \delta_{Hem}X_{Hem} + \delta_{Fe(III)\text{-}L}X_{Fe(III)\text{-}L} + \delta_{Fe(II)\text{-}L}X_{Fe(II)\text{-}L} + \delta_{Fe(II)aq}X_{Fe(II)aq} \tag{14}$$

where X is the mole fraction of various components, "Sys" refers to the total system, "Hem" refers to hematite, and "Fe(III)-L", "Fe(II)-L", and "Fe(II)aq" are defined above. Equation (14) assumes that the final product of DIR is $Fe(II)_{aq}$. We cannot use Equation (14) where the final products are magnetite and carbonate, or where there is significant quantities of surface-sorbed Fe if these components have distinct isotopic compositions (see discussion below). We may, however, simplify Equation (14) because $\delta_{Sys} = \delta_{Hem}$, and implicit in this relation is that there is no Fe isotope fractionation during the dissolution step or isotopic exchange between hematite and aqueous Fe, as discussed above. Additionally, we define the following Fe isotope fractionation factors:

$$\Delta_{Fe(III)L-Fe(II)L} = \delta_{Fe(III)\text{-}L} - \delta_{Fe(II)\text{-}L} \tag{15}$$

$$\Delta_{Fe(II)_{aq}-Fe(II)L} = \delta_{Fe(II)_{aq}} - \delta_{Fe(II)\text{-}L} \tag{16}$$

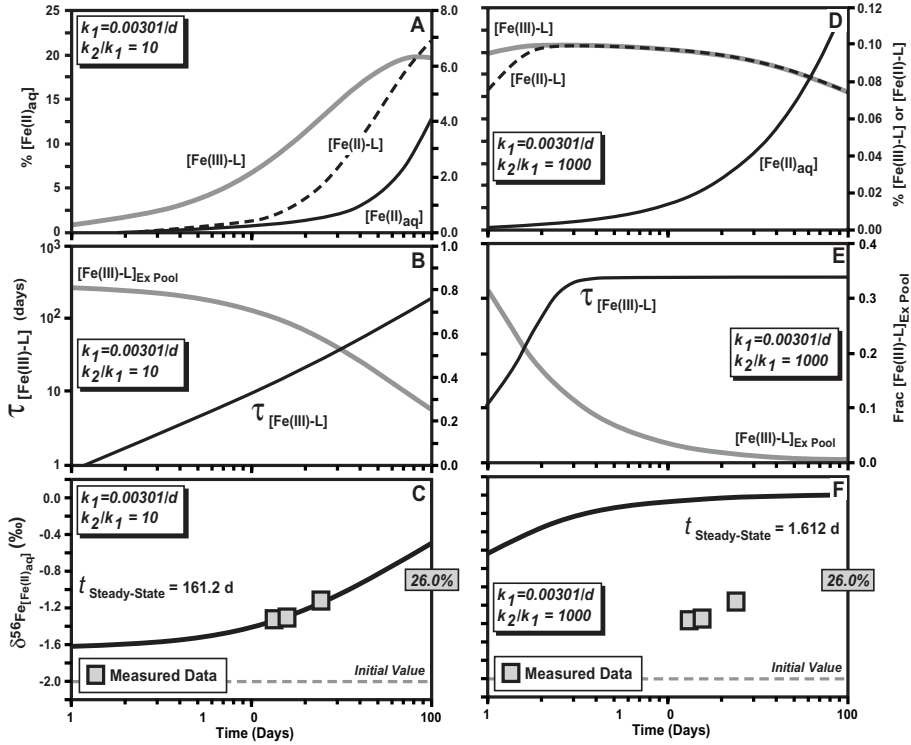

Figure 6. Reservoir sizes, residence times, and δ^{56}Fe values for aqueous Fe(II), as calculated for DIR assuming first-order rate laws. Timescale arbitrarily set to 100 days. Calculations based on rate constant k_1 determined for a 23 day DIR experiment involving hydrous ferric oxide (HFO) by *S. algae* (Beard et al. 1999). The percent total reduction at 100 days is shown in the grey box on the lower right side of the lower diagrams, based on the value of k_1. Parts A-C assume a k_2/k_1 ratio of 10, whereas parts D-F assume a k_2/k_1 ratio of 1000. As constrained by first-order rate laws, the proportion of the intermediate products Fe(III)-L, followed by Fe(II)-L, increase before substantial accumulation of the final $Fe(II)_{aq}$ product (Parts A and D). The fraction of Fe(III)-L in the exchangeable pool of Fe (Fe(III)-L + Fe(II)-L + $Fe(II)_{aq}$) decreases with time, primarily due to accumulation of the $Fe(II)_{aq}$ end product, where the rate of change is a function of the k_2/k_1 ratio.

Left panels (A-C): Where the k_2/k_1 ratio is 10, the system will not reach steady-state until 161.2 days, producing large changes in the residence time (τ) of Fe(III)-L; however, for virtually all time periods, the residence time of Fe(III)-L is several orders of magnitude longer than the time required for isotopic exchange, indicating that isotopic equilibrium will be maintained among the exchangeable pool of Fe, despite the fact that steady-state conditions are not attained when the k_2/k_1 ratio is 10. The difference in predicted δ^{56}Fe values for ferrihydrite substrate and aqueous Fe(II) are similar to those measured by Beard et al. (1999) if the Fe(III)-L - Fe(II)-L fractionation is +2.0‰.

Right panels (D-F): For a k_2/k_1 ratio of 1000, the system reaches steady-state conditions in 1.6 days. The proportion of Fe(III)-L in the exchangeable pool is exceedingly small under steady-state conditions and at high k_2/k_1 ratios, resulting in a shift in the isotopic mass balance such that the predicted δ^{56}Fe values for ferrihydrite substrate and aqueous Fe(II) are far from the inferred Fe(III)-L - Fe(II)-L fractionation.

Note that Equation (15) is the parameter that is of primary interest in this discussion, and the ultimate goal is determining the relation between the measured δ^{56}Fe value for $Fe(II)_{aq}$ and the true $\Delta_{Fe(III)L\text{-}Fe(II)L}$ fractionation, which is not measured directly. Substitution of the fractionation factors into Equation (14) produces:

$$\delta_{Fe(II)aq} = \delta_{Hem} - \frac{X_{Fe(III)\text{-}L}\,\Delta_{Fe(III)L\text{-}Fe(II)L} - \Delta_{Fe(II)aq\text{-}Fe(II)L}\left(X_{Fe(III)L} + X_{Fe(II)L}\right)}{X_{Fe(III)L} + X_{Fe(II)L} + X_{Fe(II)aq}} \quad (17)$$

We will further assume that $\Delta_{Fe(II)aq\text{-}Fe(II)L}$ is zero, that is, there is no Fe isotope fractionation between Fe(II)-$L_{Fe(II)}$ and $Fe(II)_{aq}$. This is primarily for convenience, but is equivalent to letting Fe(II)-$L_{Fe(II)}$ and $Fe(II)_{aq}$ be the same species. Setting $\Delta_{Fe(II)aq\text{-}Fe(II)L}$ to zero, and re-arrangement into measured quantities (δ_{Hem} and $\delta_{Fe(II)aq}$) on the left side, produces:

$$\delta_{Hem} - \delta_{Fe(II)aq} = \frac{X_{Fe(III)\text{-}L}\Delta_{Fe(III)L\text{-}Fe(II)L}}{X_{Fe(III)L} + X_{Fe(II)L} + X_{Fe(II)aq}} \quad (18)$$

Equation (18) illustrates that the measured δ^{56}Fe value for $Fe(II)_{aq}$ is dependent not only on $\Delta_{Fe(III)L\text{-}Fe(II)L}$, but on the proportion of Fe(III)-$L_{Fe(III)}$ in the components that are open to isotopic exchange, which additionally includes Fe(II)-$L_{Fe(II)}$ and $Fe(II)_{aq}$; we will refer to these three components as the "exchangeable pool" of Fe in the system. We stress that the isotopic mass balance described by Equation (18) assumes that the ligand-bound Fe(III) component is not sampled in the aqueous phase component, but instead exists as a component that is bound to the cells.

Temporal changes in reservoir sizes and isotopic compositions

Figure 6 illustrates the proportions of Fe(III)-$L_{Fe(III)}$, Fe(II)-$L_{Fe(II)}$, and $Fe(II)_{aq}$ using the rate constants (k_1) determined for the experiments of Beard et al. (1999). Because k_2 is unknown, we illustrate two examples, arbitrarily setting the ratio k_2/k_1 to 10 and 1000. The system will not reach steady-state in terms of the concentration ratio [HFO]/[Fe(III)-$L_{Fe(III)}$] until 161.2 days (when $k_2/k_1 = 10$) using the criterion of Equation (13), well past the length of the 23 day experiment (Fig. 6). However, during the 23-day run, the residence time for Fe(III)-$L_{Fe(III)}$ varies from ~1 day to ~100 days if $k_2/k_1 = 10$, which exceeds the time required for isotopic exchange (t_{ex}) by several orders of magnitude, even if we assume that t_{ex} is relatively long if strong organic ligands are involved. In the case of $k_2/k_1 = 1000$, the system will reach steady-state in 1.6 days, which is reflected in establishment of a constant residence time early in the experiment (Fig. 6), commensurate with the invariant $M_{Fe(III)\text{-}L}/J_{Fe(III)\text{-}L}$ ratio (Eqn. 9) under steady-state conditions.

Based on Equation (18), we expect the calculated variations in the δ^{56}Fe value for $Fe(II)_{aq}$ to be related to the fraction of Fe(III)-$L_{Fe(III)}$ in the exchangeable pool, where the difference between the measured δ^{56}Fe value for the ferric substrate and $Fe(II)_{aq}$ will most closely reflect the isotopic fractionation between Fe(III)-$L_{Fe(III)}$ and Fe(II)-$L_{Fe(II)}$ as the fraction of Fe(III)-$L_{Fe(III)}$ in the exchangeable pool (Fe(III)-$L_{Fe(III)}$ + Fe(II)-$L_{Fe(II)}$ + $Fe(II)_{aq}$) approaches unity; this condition will exist at the start of an experiment. For example, in the case of the HFO reduction experiment of Beard et al. (1999), the calculated fraction of Fe(III)-$L_{Fe(III)}$ in the exchangeable pool varies from ~0.8 at 1 day to ~0.25 at 100 days, which corresponds to changes in the δ^{56}Fe value for $Fe(II)_{aq}$ from −1.6‰ at 1 day to −0.5‰ at 100 days (Fig. 6). These calculations assume that the $\Delta_{Fe(III)L\text{ - }Fe(II)L}$ fractionation was +2.0‰, which produces δ^{56}Fe values for the measured $Fe(II)_{aq}$ component that reasonably describe the observed data (Fig. 6). The variations in the relative proportions of species in the soluble Fe pool indicate that the measured quantity $\delta_{HFO/Hem}$-$\delta_{Fe(II)aq}$ may deviate significantly from $\Delta_{Fe(III)L\text{-}Fe(II)L}$, preventing a precise estimate of the Fe isotope fractionation between Fe(III)-$L_{Fe(III)}$ and Fe(II)-$L_{Fe(II)}$.

Two important observations may be made from the calculations illustrated in Figure 6. First, isotopic equilibrium should be maintained between Fe(III)-$L_{Fe(III)}$ and Fe(II)-$L_{Fe(II)}$ despite the generally large changes that occur in their relative proportions prior to reaching steady-state conditions because the residence times of Fe in the exchangeable pools are many orders of magnitude longer than the expected time required for isotopic exchange. The second observation is that the measured quantity $\delta_{HFO/Hem}$-$\delta_{Fe(II)aq}$ only lies close to the isotopic fractionation between Fe(III)-$L_{Fe(III)}$ and Fe(II)-$L_{Fe(II)}$ at low total % reaction, when the system is actually very far from steady-state conditions, and where the proportion of Fe(III)-$L_{Fe(III)}$ in the exchangeable pool is high. If the time required for isotopic exchange is short, as expected for soluble components, then isotopic equilibrium will be maintained among the Fe(III)-$L_{Fe(III)}$, Fe(II)-$L_{Fe(II)}$, and $Fe(II)_{aq}$ components even early in the experiment. The true $\Delta_{Fe(III)L\text{-}Fe(II)L}$ fractionation may be significantly larger, however, than the measured differences in the $\delta^{56}Fe$ values for the ferric substrate and $Fe(II)_{aq}$.

Sorption effects

Sorption of $Fe(II)_{aq}$ to the ferric oxide/hydroxide starting material (substrate) may represent a significant proportion of total Fe(II) that is produced during DIR, particularly in the early stages of Fe(III) reduction (e.g., Burgos et al. 2002; Zachara et al. 2002). In addition, sorption of $Fe(II)_{aq}$ may occur on the surfaces of bacteria (e.g., Urrutia et al. 1998; Liu et al. 2001; Roden and Urrutia 2002). Icopini et al. (2004) investigated Fe isotope fractionation upon abiotic sorption of $Fe(II)_{aq}$ to goethite under anaerobic conditions. Sorption occurred rapidly, where after 24 hours, ~39% of the initial $Fe(II)_{aq}$ was sorbed to goethite. Based on isotopic analyses of the initial $FeCl_2$ reagent and $Fe(II)_{aq}$ after sorption, the $Fe(II)_{sorbed}$-$Fe(II)_{aq}$ fractionation calculated from mass balance was estimated at +2.1‰. These results are important because they suggest that sorption may play an important role in producing low $\delta^{56}Fe$ values for $Fe(II)_{aq}$ that is produced during DIR. Icopini et al. (2004) concluded that a large component of the fractionation observed between $Fe(II)_{aq}$ and ferric oxide/hydroxide substrates in DIR experiments may occur by entirely abiotic means, which stands in contrast to the model discussed above where the major fractionation step is inferred to occur between ligand-bound pools of Fe(III) and Fe(II).

A different view on the role of Fe(II) sorption during DIR was presented by Johnson et al. (2004a), who suggested that early rapid sorption of $Fe(II)_{aq}$ during the initial stages of DIR is accompanied by significant kinetic isotope fractionation, followed by approach toward isotopic equilibrium over longer timescales, when the $Fe(II)_{sorbed}$-$Fe(II)_{aq}$ fractionation converges toward zero. Because the $\delta^{56}Fe$ values of $Fe(II)_{aq}$ was correlated with Fe reduction rates (Fig. 7), where the lowest values occurred when the major repository of Fe(II) existed as sorbed Fe, Johnson et al. (2004a) estimated that the initial kinetic fractionation between $Fe(II)_{sorbed}$ and $Fe(II)_{aq}$ during sorption was ~2‰ or larger, which is similar to that observed by Icopini et al. (2004). HFO was progressively converted to lepidocrocite over time in an experiment using *Geobacter sulfurreducens* in the study of Johnson et al. (2004a), such that the major proportion of HFO, if not all, was converted within ~16 days. The solid phase conversion was likely accompanied by a large reduction in surface area, which released isotopically heavy Fe that had been sorbed early in the experiment. At relatively low Fe reduction rates, the isotopic contrast between $Fe(II)_{aq}$ and ferric oxyhydroxide substrate approached that observed in longer-term experiments (Fig. 7), which Johnson et al. (2004a) inferred to reflect the equilibrium fractionation between ligand-bound Fe(III) and Fe(II) and a zero fractionation between sorbed Fe(II) and $Fe(II)_{aq}$. Johnson et al. (2004a) note that if abiotic sorption is the primary explanation for the low $\delta^{56}Fe$ values observed for $Fe(II)_{aq}$ during DIR, as argued by Icopini et al. (2004), this suggests that the fractionation between any ligand-bound Fe(III) and Fe(II) components ("Fe(III)-$L_{Fe(III)}$" and "Fe(II)-$L_{Fe(II)}$" in Fig. 5) must be near zero, which seems unlikely given the major effect of redox state on Fe isotope fractionations.

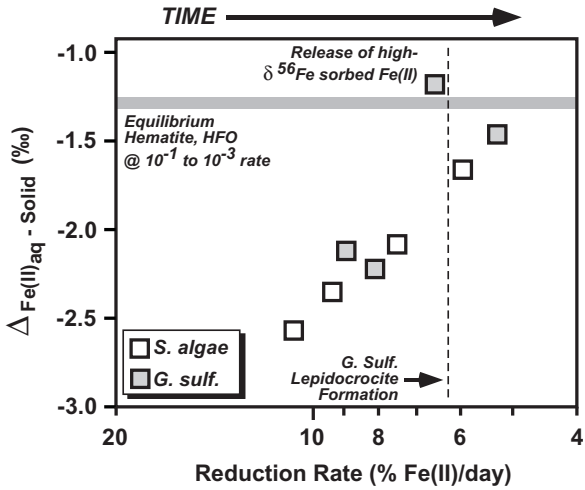

Figure 7. Changes in the fractionation between $Fe(II)_{aq}$ and the solid ferric hydroxide substrate for a comparative study of DIR by *G. sulfurreducens* and *S. algae*, as a function of Fe reduction rates. Reduction rate plotted as decreasing to the right, which reflects increasing time. The initial ferric hydroxide substrate is HFO, which undergoes phase conversion to lepidocrocite in the *G. sulfurreducens* experiment by the end of the third time sample. The decrease in $\Delta_{Fe(II)aq\text{-}Solid}$ fractionations with decreasing Fe reduction rates are interpreted by Johnson et al. (2004a) to reflect an early, large-magnitude fractionation due to kinetic effects upon rapid sorption of Fe(II), followed by an approach to isotopic equilibrium with time. The large decrease in sorption capacity during conversion of HFO to lepidocrocite that occurs in the *G. sulfurreducens* experiment is accompanied by an increase in the $\delta^{56}Fe$ value for $Fe(II)_{aq}$, producing a decrease in the magnitude of the $\Delta_{Fe(II)aq\text{-}Solid}$ fractionation. The equilibrium fractionation between $Fe(II)_{aq}$ and ferric substrate is taken to be that measured in the experiments of Beard et al. (1999, 2003a), which involved much slower Fe reduction rates (10^{-1} to 10^{-3} % Fe(II)/day). Modified from Johnson et al. (2004a).

The isotopic effects of sorption may also be explored using mass-balance relations between sorbed and aqueous Fe. If, for example, the isotopic fractionation observed by Icopini et al. (2004) reflects closed-system equilibrium exchange, the $\delta^{56}Fe$ value of $Fe(II)_{aq}$ should be a function of the proportion of Fe sorbed (Fig. 8). The proportion of sorbed Fe(II) may be calculated for the DIR experiments of Beard et al. (1999, 2003a) using surface areas and saturation capacities from the literature (e.g., Roden and Zachara 1996, and references within), and these, in addition to the *measured* sorption from Johnson et al. (2004a), are plotted in Figure 8, relative to mass-balance sorption lines based on the single determination by Icopini et al. (2004). Although there is some uncertainty in the calculated sorption capacities for HFO and hematite in the experiments of Beard et al. (1999, 2003a), it seems likely that the proportion of sorbed Fe(II) must have been quite different among these studies, and yet all produced similar $\delta^{56}Fe$ values for $Fe(II)_{aq}$ (Fig. 8). If the isotopic fractionations determined by Beard et al. (1999, 2003a) and Johnson et al. (2004a) reflected only sorption of $Fe(II)_{aq}$ and a +2.1‰ $Fe(II)_{Sorbed}$-$Fe(II)_{aq}$ fractionation (Icopini et al. 2004), the data should lie along the diagonal mass-balance lines if closed-system equilibrium fractionation describes the process; instead, they have a relatively constant $\delta^{56}Fe$ values for $Fe(II)_{aq}$ over a wide range of % sorption.

The isotopic effects of sorption remain relatively unknown, with disparate interpretations of its significance during DIR. An important avenue of future research will be to quantify the rates of isotopic exchange between sorbed Fe(II) and $Fe(II)_{aq}$, and to investigate a range of ferric oxide/hydroxide substrates. Because traditional sorption experiments generally

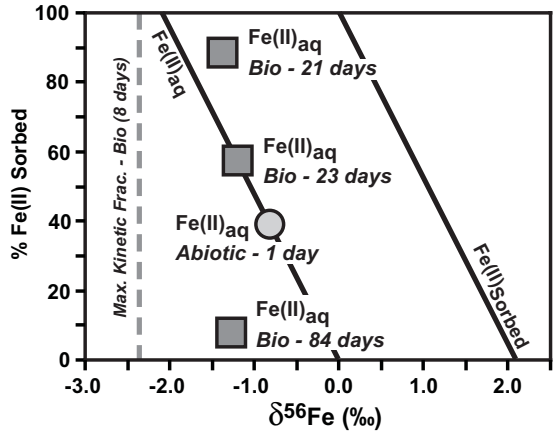

Figure 8. Isotopic mass-balance relations between sorbed Fe(II) and fraction of Fe sorbed for abiotic sorption experiment of Icopini et al. (2004) and those calculated for long-term DIR experiments of Beard et al. (1999, 2003a) and Johnson et al. (2004a). The lowest δ^{56}Fe value for $Fe(II)_{aq}$ measured by Johnson et al. (2004a) is shown by the vertical dashed line, which is interpreted to be a kinetic effect due to rapid sorption. Data normalized to a system δ^{56}Fe value of zero to aid in comparison. Measured data for $Fe(II)_{aq}$ after sorption shown in light gray circle for study of Icopini et al. (2004), and solid diagonal lines indicate calculated isotopic mass balance from that study, assuming a closed-system equilibrium model. Measured data for $Fe(II)_{aq}$ from DIR studies of Beard et al. (1999, 2003a) shown in dark gray squares. Percent Fe(II) sorbed for experiment by Johnson et al. (2004a) is calculated from the measured total and $Fe(II)_{aq}$ contents; if calculated using measured $Fe(II)_{aq}$ contents and an assumed surface area of 600 m^2/g and capacity of 3×10^{-6} mol/g, the% sorbed Fe(II) is 83.8% instead of the 89.0% based on the measured data. Percent Fe(II) sorbed for the experiments of Beard et al. (1999, 2003a) calculated using measured $Fe(II)_{aq}$ contents and assuming surface areas for HFO and hematite of 600 m^2/g and 5 m^2/g, respectively, and capacity of 3×10^{-6} mol/g. A factor of 2 change in surface area correlates with a 6% (hematite) and 17% (HFO) change in the % Fe(II) sorbed.

involve very rapid uptake from high-Fe(II) solutions (e.g., Burgos et al. 2002), which are conditions that are far from the very slow Fe(II) production rates that were associated with the DIR experiments of Beard et al. (1999, 2003a), as well as DIR in nature (e.g., Glausauer et al. 2003), constraining the kinetic effects of sorption will be important. If the equilibrium isotope fractionation between sorbed and aqueous Fe(II) is near zero as suggested by Johnson et al. (2004a), then a sorption term does not need to be introduced into Equations (5)–(8). If, however, early kinetic isotope fractionation occurs during rapid DIR, then the equations would need to be modified, although they may still be applicable to slow rates of DIR where isotopic equilibrium may be approached.

Solid products of DIR

A wide variety of solid products may form during DIR (Table 2). Magnetite readily forms through reaction of soluble Fe(II) that is produced during DIR with the ferric substrate (e.g., Lovley et al. 1987; Roden and Lovely 1993; Fredrickson et al. 1998; Zachara et al. 2002). *G. sulfurreducens*, for example, produces magnetite and siderite as primary end-products of synthetic HFO reduction when a bicarbonate-buffered medium is used (e.g., Caccavo et al. 1994; Lloyd et al. 2000). Recent studies have demonstrated that production of siderite occurs during HFO reduction by *Shewanella putrefaciens* strain CN32, without formation of magnetite (Fredrickson et al. 1998; Parmar et al. 2000; Roden et al. 2002). We first focus on the results of experimental studies where a single phase was produced because of the additional complexities in interpreting Fe isotope fractionations where multiple solid phases are formed.

Production of solid phases during DIR may be highly path dependent, determined by bacterial species and experimental conditions such as growth media and ferric substrate. Because formation of the solid phases during DIR is analogous to mineral synthesis experiments, the same uncertainties exists in interpreting measured fluid-mineral isotope fractionations in terms of kinetic or equilibrium effects as are present in abiologic synthesis experiments (e.g., Chapter 1; Johnson et al. 2004b). For example, large crystals that formed during early rapid precipitation may record highly variable Fe isotope compositions because they may not have been in isotopic equilibrium with aqueous Fe when they formed, and may not fully respond to changes in the Fe isotope composition of the aqueous phase with time due to limited solid-state equilibration or dissolution/re-precipitation at low temperatures. Fine-grained crystals, or the outer portions of large crystals, however, may be closer to isotopic equilibrium with the aqueous phase if they are actively undergoing dissolution and re-precipitation, provided that such processes occurred sufficiently slowly so as to maintain isotopic equilibrium.

Calculated and measured Fe isotope fractionation factors between $Fe(II)_{aq}$ and magnetite vary between −4 and 0‰ (Fig. 9), which is a significant range given the few per mil variations seen in chemically precipitated sediments to date (Beard and Johnson 1999; Zhu et al. 2000; Johnson et al. 2003; Matthews et al. 2004). The largest magnitude $\Delta_{Fe(II)\text{-}Magnetite}$ fractionation, −4.2‰ (Fig. 9), is calculated from spectroscopic data, using the reduced partition function ratios (β factors) from Polyakov and Mineev (2000) and Schauble et al. (2001). A more

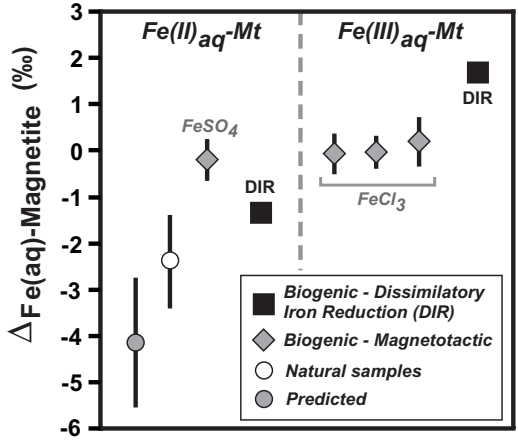

Figure 9. Comparison of isotopic fractionations between Fe in solution ($Fe(II)_{aq}$ and $Fe(III)_{aq}$) and magnetite from predictions based on spectroscopic data (Polyakov and Mineev 2000; Schauble et al. 2001), natural samples (Johnson et al. 2003), and experimental studies of biogenic magnetite formation (Mandernack et al. 1999; Johnson et al. 2004a). Error bars shown reflect estimated uncertainties from specific studies; analytical errors for data reported for DIR by Johnson et al. (2004a) are smaller than the size of the symbol. $Fe(II)_{aq}$–magnetite fractionations shown on left side of figure, and $Fe(III)_{aq}$ - magnetite fractionations shown on right side of figure. The measured $Fe(II)_{aq}$–magnetite fractionation in the DIR study also has been converted to $Fe(III)_{aq}$–magnetite using the $Fe(III)_{aq}$–$Fe(II)_{aq}$ fractionation reported by Johnson et al. (2002) and Welch et al. (2003), so that these results may be compared to the $Fe(III)_{aq}$–magnetite fractionations measured for magnetotactic bacteria by Mandernack et al. (1999). The results for DIR contrast strongly with those calculated from spectroscopic data, but just overlap those predicted using natural data, within the estimated uncertainties. Isotopic fractionations measured by Johnson et al. (2004a) are significantly different, however, from those measured by Mandernack et al. (1999) for magnetotactic bacteria; the later also show unexplained inconsistencies between $Fe(II)_{aq}$–magnetite and $Fe(III)_{aq}$–magnetite fractionations. Adapted from Johnson et al. (2004a).

moderate $\Delta_{Fe(II)\text{-}Magnetite}$ fractionation of approximately −2.4‰ (Fig. 9) is calculated using natural samples (Johnson et al. 2003) and the $Fe(II)_{aq}$ β factor from Schauble et al. (2001), and this fractionation more closely matches that estimated to be produced during DIR (Johnson et al. 2004a). The $Fe(II)_{aq}$ - magnetite fractionation factor measured by Johnson et al. (2004a) during DIR is interpreted to reflect an equilibrium isotope fractionation based on experimental runs that produced simple solid phase assemblages and isotopically homogeneous crystals as determined by partial dissolutions. The Fe isotope fractionations measured in the study of magnetite formation by DIR are, however, significantly different from those measured for magnetotactic bacteria (Fig. 9; Mandernack et al. 1999).

It is unclear if the $\Delta_{Fe(II)aq\text{-}Magnetite}$ fractionations that were measured for magnetite formation by magnetotactic bacteria (Mandernack et al. 1999) reflect equilibrium conditions because of inconsistencies in the $Fe(II)_{aq}$–magnetite and $Fe(III)_{aq}$–magnetite fractionations (Fig. 9). For example, Mandernack et al. (1999) report similar $Fe(II)_{aq}$–magnetite and $Fe(III)_{aq}$–magnetite fractionations, which is not at all expected if the experimental conditions reflected equilibrium conditions, given the +2.9‰ fractionation between $[Fe^{III}(H_2O)_6]^{3+}$ and $[Fe^{II}(H_2O)_6]^{2+}$ in solution (Johnson et al. 2002; Welch et al. 2003). Using the experimentally determined $Fe(III)_{aq}$–$Fe(II)_{aq}$ fractionation, recalculation of the estimated equilibrium $Fe(II)_{aq}$–magnetite fractionation measured in the study of Johnson et al. (2004a) to $Fe(III)_{aq}$–magnetite produces $\Delta_{Fe(III)\text{-}Magnetite} = +1.7‰$, which stands in marked contrast to that measured for three experiments using $Fe(III)Cl_3$ by Mandernack et al. (1999) (Fig. 9). Calculation of $\Delta_{Fe(III)\text{-}Magnetite}$ by this method assumes isotopic equilibrium exists between $Fe(III)_{aq}$ and magnetite, independent of the pathways in which isotopic equilibrium may be attained in a system that contains mixed valance states of Fe. Most of the magnetotactic experiments were done at 28°C, which produced very rapid formation of magnetite, and a possible explanation is that the measured isotope fractionations reflect kinetic isotope effects.

The equilibrium $\Delta_{Fe(II)aq\text{-}Fe\ Carbonate}$ fractionation for pure siderite during DIR is estimated to be near zero, and that for Ca-bearing Fe carbonates is ≥1‰ (Fig. 10) (Johnson et al. 2004a). In contrast, kinetic $\Delta_{Fe(II)aq\text{-}Fe\ Carbonate}$ fractionations produced during DIR are ~1‰ higher than those estimated for equilibrium fractionations, for both pure siderite and Ca-bearing siderite (Fig. 10). A wide range in $Fe(II)_{aq}$–Fe-carbonate fractionations are predicted from spectroscopic and natural data, spanning values from −0.7 to +3.5‰ (Fig. 10; Polyakov and Mineev 2000; Schauble et al. 2001; Johnson et al. 2003). The equilibrium $Fe(II)_{aq}$–siderite fractionation in abiotic systems is estimated at +0.5‰ (Fig. 10; Wiesli et al. 2004), which is somewhat larger than that estimated from DIR experiments. The $Fe(II)_{aq}$–Fe-carbonate fractionations inferred from natural mineral assemblages and those predicted from theory suggest that the $\Delta_{Fe(II)aq\text{-}Fe\ carbonate}$ fractionations should increase with decreasing mole fraction of Fe, from "siderite" to "ankerite" (Fig. 10). The effect of increasing $\Delta_{Fe(II)aq\text{-}Fe\ carbonate}$ upon Ca substitution was observed by Johnson et al. (2004a), suggesting that the bonding changes and distortions in the crystal lattice that accompany even small amounts of Ca substitution into siderite produce significant Fe isotope effects. Because natural Fe carbonates commonly contain significant Ca, Mn, and Mg, it seems likely that carbonate stoichiometry may exert a substantial control on Fe isotope fractionations between $Fe(II)_{aq}$ and carbonate, and it is anticipated that this will be seen in both biologic and abiotic systems.

In addition to producing biogenic magnetite and siderite during DIR, formation of poorly crystalline Fe(II)-bearing solid phases commonly occurs (Table 2), and these may be difficult to detect using XRD spectra. Partial dissolution of solids using weak acids has been used to isolate non-magnetic, non-carbonate Fe(II) solids (e.g., Fredrickson et al. 1998; Roden et al. 2002), and such approaches may also be used to isolate such components for isotopic analysis (Johnson et al. 2004a). Treatments with weak acids may also, however, dissolve unreduced ferric oxide/hydroxide substrates or sorbed Fe components, and determination of Fe(III) and

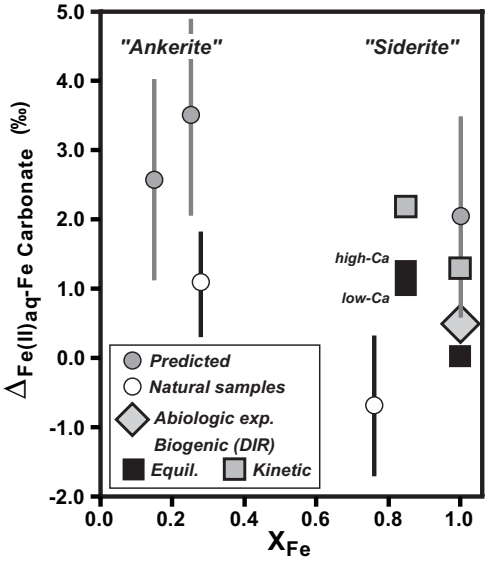

Figure 10. Comparison of isotopic fractionations determined between $Fe(II)_{aq}$ and Fe carbonates relative to mole fraction of Fe from predictions based on spectroscopic data (Polyakov and Mineev 2000; Schauble et al. 2001), natural samples (Johnson et al. 2003), DIR (Johnson et al. 2004a), and abiotic formation of siderite under equilibrium conditions (Wiesli et al. 2004). $Fe(II)_{aq}$ exists as the hexaquo complex in the study of Wiesli et al. (2004); hexaquo Fe(II) is assumed for the other studies. Total cations normalized to unity, so that end-member siderite is plotted at $X_{Fe} = 1.0$. Error bars shown reflect reported uncertainties; analytical errors for data reported by Johnson et al. (2004a) and Wiesli et al. (2004) are smaller than the size of the symbol. Fractionations measured on bulk carbonate produced by DIR are interpreted to reflect kinetic isotope fractionations, whereas those estimated from partial dissolutions are interpreted to lie closer to those of equilibrium values because they reflect the outer layers of the crystals. Also shown are data for a Ca-bearing DIR experiment, where the bulk solid has a composition of approximately $Ca_{0.15}Fe_{0.85}CO_3$, "high-Ca" and "low-Ca" refer to the range measured during partial dissolution studies (Johnson et al. 2004a). Adapted from Johnson et al. (2004a).

Fe(II) contents of the material that has been partially dissolved is required to confidently identify the solid components that have been sampled. In the DIR experiments of Johnson et al. (2004a), significant quantities of a non-magnetic, non-carbonate Fe(II)(s) phase, which we will refer to as NMNC Fe(II)(s), were produced under some conditions, and this phase may exert a strong influence on the Fe isotope compositions of $Fe(II)_{aq}$. In cases where rapid formation of NMNC Fe(II)(s) occurs early, such material appears to have very low $\delta^{56}Fe$ values relative to those of $Fe(II)_{aq}$, driving the remaining $Fe(II)_{aq}$ to very high $\delta^{56}Fe$ values (Johnson et al. 2004a). In contrast, slow production of small quantities of NMNC Fe(II)(s) appears to have $\delta^{56}Fe$ values that are similar to those of $Fe(II)_{aq}$, suggesting that the equilibrium fractionation between NMNC Fe(II)(s) and $Fe(II)_{aq}$ is near zero (Johnson et al. 2004a).

The isotopic effects of DIR using Fe(III)-bearing clay minerals are unknown, but represent an important avenue of future research. Reduction of smectite by DIR bacteria produces significant changes in clay structures (e.g., Kostka et al. 1999a,b). In addition, DIR may catalyze phase transformations in clay minerals, such as conversion of smectite to illite (Kim et al. 2004). The very high surface areas of clay minerals, as well as their high sorption capacity, suggest that there may be significant Fe isotope fractionations during DIR involving Fe(III)-bearing clay minerals as the terminal electron acceptor.

Summary of Fe isotope fractionations produced during DIR

The Fe isotope fractionations that have been observed to date in experimental studies of DIR are summarized in Figure 11. The isotopic compositions are calculated using the fractionation factors listed in Table 3, setting the δ^{56}Fe value of the ferric substrate starting material (HFO, goethite, hematite, etc.) or magnetite solid product to zero, consistent with the general observation that Fe mass balance is dominated by these phases in DIR experiments. During the initial stages of reduction and over short time periods, the δ^{56}Fe values for $Fe(II)_{aq}$, NMNC Fe(II)(s), and sorbed Fe(II) are interpreted to largely reflect kinetic isotope fractionations. Note, however, that although any ligand-bound Fe(III) components might be in isotopic equilibrium with $Fe(II)_{aq}$, based on the long residence times that are calculated (e.g., Fig. 6), the δ^{56}Fe values for $Fe(II)_{aq}$ are likely to be controlled by rapid formation of other components at early stages. These components may include sorbed Fe(II) and NMNC Fe(II)(s). If early, rapid sorption of $Fe(II)_{aq}$ produces a kinetic isotope fractionation that results in anomalously low δ^{56}Fe values for $Fe(II)_{aq}$, this is opposite the effect that is produced by rapid precipitation of NMNC Fe(II)(s). The net changes in δ^{56}Fe values for $Fe(II)_{aq}$ during the initial stages of rapid DIR are therefore likely to be strongly dependent on the relative rates of Fe(II) sorption and formation of NMNC Fe(II)(s).

The general progression in importance of sorbed Fe(II) to NMNC Fe(II)(s) illustrated in Figure 11 follows that observed in experimental studies. The changes in isotopic fractionations between $Fe(II)_{aq}$ and NMNC Fe(II)(s) are well documented by partial dissolutions of the solid phases produced during DIR (Johnson et al. 2004a). The inferred changes in $Fe(II)_{aq}$–$Fe(II)_{sorbed}$ fractionations, however, are less well constrained and this component of DIR needs further study, as noted above. For simplicity, we have omitted Fe carbonate as a solid product in Figure 11, but note that similar changes in isotopic fractionation between $Fe(II)_{aq}$ and solid are inferred to occur, recording initial kinetic conditions that existed during rapid reduction, as well as movement toward equilibrium with time (Johnson et al. 2004a). Finally, we note that besides magnetite, many of the components illustrated in Figure 11 have negative δ^{56}Fe values, suggesting that there is a missing, relatively high-δ^{56}Fe component that has not been analyzed in these experiments. Following the model developed above (Fig. 6), we assume this high-δ^{56}Fe component is a reservoir of Fe(III), which we termed "Fe(III)-$L_{Fe(III)}$" to refer to a ligand- or cell-bound Fe(III) component that would not be present in samples of $Fe(II)_{aq}$ or other Fe-bearing solids that are analyzed in a typical experiment.

ANAEROBIC PHOTOSYNTHETIC Fe(II) OXIDATION

Investigation of Fe isotope fractionation produced by anaerobic photosynthetic Fe(II) oxidation is much less extensive than it is for DIR. Possible pathways where Fe isotopes may be fractionated during anaerobic photosynthetic Fe(II) oxidation, which we will refer to as APIO, are illustrated in Figure 12. There are four possible steps in which Fe isotope fractionation may occur (Croal et al. 2004). Isotopic fractionation may occur during binding of Fe from the ambient aqueous $Fe(II)Cl_2$ starting material to a redox-active site or ligand. Because there is no change in oxidation state at this stage, however, it is anticipated that Fe isotope fractionation, if any, will be relatively small for this step. Iron oxidation occurs in the next step (Fig. 12), and Croal et al. (2004) postulate that a significant step in which Fe isotope fractionation may occur is between ligand-bound Fe(III) and Fe(II) (Δ_1, Fig. 12), given the fact that relatively large Fe isotope fractionations occur between Fe(III) and Fe(II) phases. Isotopic fractionation at this step in the model of Figure 12 is similar to that illustrated for DIR in Figure 5, although the process is occurring in the opposite direction, and, as will be discussed below, likely involves different pools of exchangeable Fe. Formation of the final ferric hydroxide end products may also be accompanied by Fe isotope fractionation, which is essentially an isotopic fractionation upon precipitation (Δ_2, Fig. 12). Finally, it is possible that

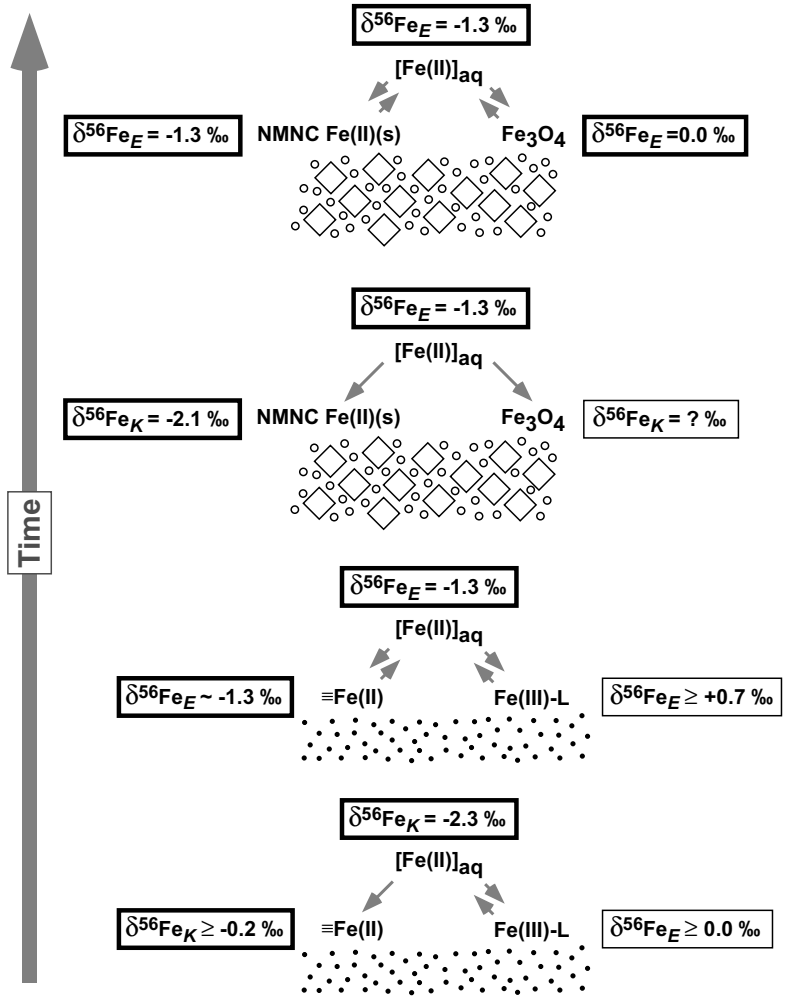

Figure 11. Summary of Fe isotope fractionations produced during DIR, based on isotopic fractionations factors in Table 3. δ^{56}Fe values for measured species shown by boxes with heavy lines, and those that are inferred for species not directly measured shown by boxes with thin lines. Isotopic compositions calculated assuming the δ^{56}Fe values for ferric oxide/hydroxide substrate and magnetite equal zero. During the initial stages of DIR (bottom figure), when Fe reduction rates are highest, rapid formation of $Fe(II)_{aq}$ results in rapid sorption to the ferric oxide/hydroxide substrate (small solid dots), producing very low δ^{56}Fe values that are interpreted to reflect kinetic isotope fractionation. At later stages of DIR, when Fe reduction rates are slower, but prior to formation of significant quantities of reduced solid products (second from bottom figure), the δ^{56}Fe values of $Fe(II)_{aq}$ are interpreted to reflect equilibrium fractionation between ligand-bound Fe(III) and $Fe(II)_{aq}$, and the δ^{56}Fe value of sorbed Fe(II) is inferred to be similar to that of $Fe(II)_{aq}$. Formation of significant quantities of Fe(II)-bearing solid products is illustrated in the third from the bottom figure, including magnetite (Fe_3O_4) in diamonds and non-magnetic, non-carbonate Fe(II)(s) [NMNC Fe(II)(s)] in small open circles; the later phase, if formed rapidly, is interpreted to have very low δ^{56}Fe values that reflect kinetic isotope fractionation. Over the long term, when the system more closely reflects equilibrium conditions (top figure), the isotopic effects of NMNC Fe(II)(s) are minimal, and the δ^{56}Fe values of $Fe(II)_{aq}$ are interpreted to reflect equilibrium fractionation with magnetite.

Table 3. Summary of Fe isotope fractionations during biogenic mineral formation.

Species	*Kinetic* $\Delta_{A\text{-}B}$	*Equilibrium* $\Delta_{A\text{-}B}$	*Ref.*
Dissimilatory Fe(III) reduction:			
$Fe(II)_{aq}$ - $FeCO_3$	+1.2‰	+0.0‰	1
$Fe(II)_{aq}$ - $Ca_{0.15}Fe_{0.85}CO_3$	+2.2‰	+0.9‰	1
$Fe(II)_{aq}$ - Fe_3O_4		−1.3‰	1
$Fe(II)_{aq}$ - Ferric oxide/hydroxide substrate (DIR)	−2.3‰	−1.3‰	2
$Fe(II)_{aq}$ - NMNC Fe(II)(s)	+0.8‰	~0‰	1
$Fe(II)_{aq}$ - ≡Fe(II) [HFO]	−2.1‰	~0‰	3
Fe_3O_4 - $FeCO_3$	+3.5‰	+1.3‰	1
Fe_3O_4 - $Ca_{0.15}Fe_{0.85}CO_3$	+4.5‰	+2.2‰	1
Anaerobic photosynthetic Fe(II) oxidation:			
$Fe(II)_{aq}$ - Ferric oxide/hydroxide precipitate (APIO)		−1.5‰	4

References:
1 - Johnson et al. (2004a).
2 - Beard et al. (1999; 2003a); Johnson et al. (2004a).
3 - Icopini et al. (2004); Johnson et al. (2004a).
4 - Croal et al. (2004).

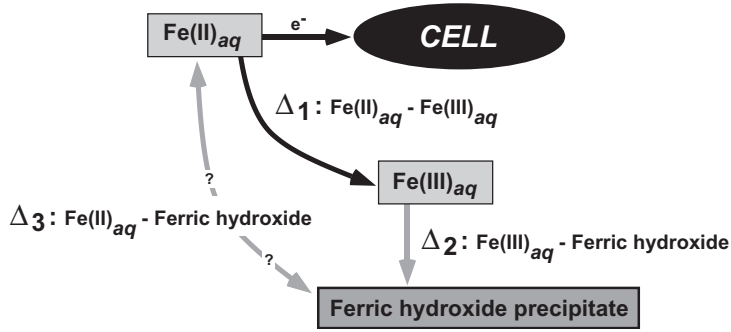

Figure 12. Possible isotope fractionation steps during anaerobic photosynthetic Fe(II) oxidation (APIO). It is assumed that the process of oxidation proceeds through an oxidation step, where $Fe(II)_{aq}$ is converted to soluble Fe(III) in close proximity to the cell, followed by precipitation as ferric oxides/hydroxides. As in DIR (Fig. 5), the most likely step in which the measured Fe isotope fractionations are envisioned to occur is during oxidation, where isotopic exchange is postulated to occur between pools of Fe(II) and Fe(III) (Δ_1). As discussed in the text and in Croal et al. (2004), however, it is also possible that significant Fe isotope fractionation occurs between $Fe(III)_{aq}$ and the ferrihydrite precipitate (Δ_2); in this case the overall isotopic fractionation measured between $Fe(II)_{aq}$ and the ferrihydrite precipitate would reflect the sum of Δ_1 and Δ_2, assuming the proportion of Fe(III) is small (see text for discussion). Isotopic exchange may also occur between $Fe(II)_{aq}$ and the ferric hydroxide precipitate (Δ_3), although this is considered unlikely.

isotopic exchange may occur between the ferric hydroxide precipitates and $Fe(II)_{aq}$ (Δ_3, Fig. 12); such exchange is most likely to occur if the precipitate is nm-size ferrihydrite, but seems unlikely if ferrihydrite consists of larger diameter crystals or is converted to more crystalline forms such as goethite, given the very low rate of isotopic exchange between aqueous Fe and oxides at low temperatures (Poulson et al. 2003).

Although there may be several steps that produce isotopic fractionation during APIO, the process is simpler in some ways than DIR in that a single solid phase is produced, and sorption effects on the isotopic composition of $Fe(II)_{aq}$ are insignificant during the early stages of oxidation when the proportion of $Fe(II)_{aq}$ to ferrihydrite precipitate is very large (Croal et al. 2004). We can describe the APIO process as:

$$Fe(II)_{aq} \rightarrow Fe(III)_{aq} \rightarrow Fe(OH)_3(s) \quad (19)$$

which is identical to that used to describe abiotic oxidation of $Fe(II)_{aq}$ in the previous chapter (Chapter 10A; Beard and Johnson 2004). Equation (19) explicitly assumes that precipitation of ferric hydroxide is preceded by formation of $Fe(III)_{aq}$. Although the overall process of APIO may appear similar to abiotic oxidation of $Fe(II)_{aq}$, the former occurs in the absence of O_2 and involves binding to biologic sites, whereas the later involves inorganic oxidation of Fe(II) by oxygen. In the case of APIO, it may be that one of more pools of soluble Fe are bound to biological ligands, where, for example, $Fe(III)_{aq}$ would be better represented as $Fe(III)\text{-}L_{Fe(III)}$. The quantities of ligand-bound Fe(III) present during APIO, however, is likely to be very small, given the very low levels of Fe(III)-specific organic ligands that have been detected (Kappler and Newman 2004). Nevertheless, the binding environments may be sufficiently distinct for soluble Fe(II) and Fe(III) during oxidation in the outer cell membrane or at the surface, as compared to simple aqueous solutions of Fe(II) and Fe(III), raising the possibility that Fe isotope fractionations produced by APIO may be distinct from those measured between $Fe(III)_{aq}$ and $Fe(II)_{aq}$ in abiotic solutions.

Proportions of reacting species

If the process of APIO is properly described by Equation (19), which infers the presence of a soluble Fe(III) intermediate species, it will be difficult to analyze this species directly, given the low levels that are expected. We must therefore develop mathematical approaches to estimating the isotopic composition of this component, as was done for DIR. The equations used in the previous chapter (Chapter 10A; Beard and Johnson 2004) to describe abiotic Fe(II) oxidation are useful for illustrating possible isotopic fractionations that may occur during APIO. We will assume that the overall oxidation process occurs through a series of first-order rate equations, where relatively slow oxidation of $Fe(II)_{aq}$ to a soluble Fe(III) component occurs, which we will denote as $Fe(III)_{aq}$ for simplicity. The oxidation step is followed by precipitation of $Fe(III)_{aq}$ to ferrihydrite at a much faster rate, which maintains a relatively low level of $Fe(III)_{aq}$ relative to $Fe(II)_{aq}$. The assumption of first-order kinetics is not strictly valid for the experiments reported in Croal et al. (2004), where decreasing $Fe(II)_{aq}$ contents with time do not closely follow either zeroth-, first-, or second-order rate laws. However, use of a first-order rate law allows us to directly compare calculations here with those that are appropriate for abiologic Fe(II) oxidation, where experimental data are well fit to a first-order rate law (Chapter 10A; Beard and Johnson 2004).

Croal et al. (2004) investigated APIO using an enrichment culture of Fe(II)-oxidizing photoautotrophs, as well as a pure culture of the genus *Thiodictyon*, which was cultured at three different light intensities (40, 80, and 120 cm distances from a 40W light source) to investigate possible kinetic effects on isotopic fractionations. Using the three different rates (k_1) that fit the extent of reactions at the end of the 20 day experiments at the three different light intensities, we calculate the relative proportions of $Fe(II)_{aq}$, $Fe(III)_{aq}$, and ferrihydrite precipitate (noted as $Fe(OH)_3(s)$ for simplicity) at various ratios of k_2/k_1 (Fig. 13). We illustrate

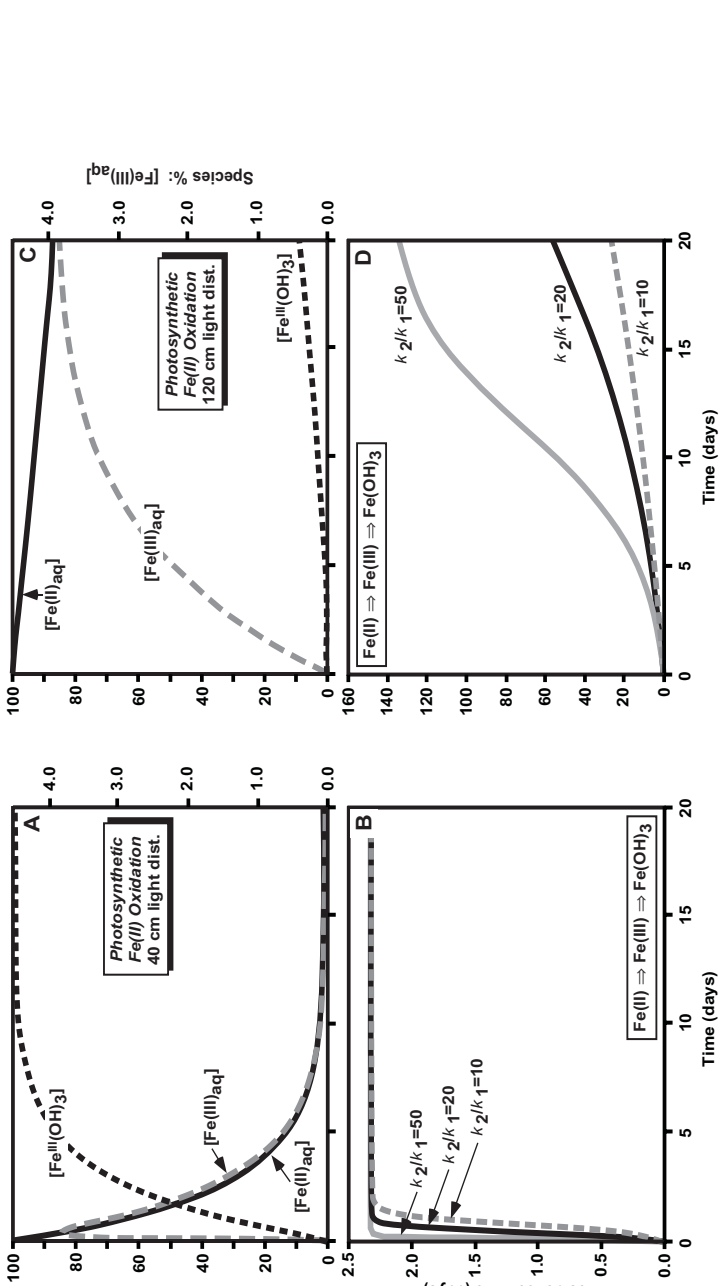

Figure 13. Proportions of Fe species during APIO, assuming first-order kinetics. The rate constant k_1 is determined using the last time points where measurable $Fe(II)_{aq}$ and ferrihydrite precipitate exist in the experiments of Croal et al. (2004). Parts A and C illustrate the proportion of components for experiments run at 40 and 120 cm distances from the light source, respectively, including $Fe(II)_{aq}$ starting material, an inferred intermediate product of $Fe(III)_{aq}$, and the final product of ferrihydrite precipitate (shown as $Fe(OH)_3$ for simplicity). Curves calculated assuming a k_2/k_1 ratio of 20. In Parts B and D, the residence time for $Fe(III)_{aq}$ is illustrated for a variety of k_2/k_1 ratios (10, 20, and 50), for experiments at 40 and 120 cm distances from the light source, respectively. If the residence time for $Fe(III)_{aq}$ is significantly longer than the time required for isotopic exchange between $Fe(II)_{aq}$ and $Fe(III)_{aq}$, the isotopic fractionation between soluble Fe(II) and Fe(III) pools (Δ_1 in Fig. 12) will reflect equilibrium Fe isotope fractionations.

calculations for several k_2/k_1 ratios (10, 20, and 50), all of which would produce small quantities of $Fe(III)_{aq}$. Oxidation rates were fastest for the experiment that involved the highest light intensity (40 cm distance), and, for a k_2/k_1 ratio of 20, steady-state conditions in terms of $Fe(II)_{aq}/Fe(III)_{aq}$ ratios would be attained in 0.56 days (Fig. 13). Under such conditions, the residence time of $Fe(III)_{aq}$ quickly reaches a maximum value of 2.3 days early in the experimental run. Such long residence times, relative to the timescales of isotopic exchange, ensures that isotopic equilibrium would have been maintained between $Fe(II)_{aq}$ and $Fe(III)_{aq}$ during the 20 day experiment. The very slow k_1 rate constant for the experiment at 120 cm light distance would prevent this experiment from attaining steady-state conditions over its 20-day timescale (Fig. 13), and therefore the residence time for $Fe(III)_{aq}$ would not reach its maximum prior to termination of the experiment. We calculate, however, that during virtually the entire experiment the residence time of $Fe(III)_{aq}$ would be on the order of days for the experiments run at distances of 80 and 120 cm from the light source, indicating that isotopic equilibrium should have been maintained between $Fe(II)_{aq}$ and $Fe(III)_{aq}$.

Constraints on isotopic variations

Using simple mass-balance relations, we may calculate the $\delta^{56}Fe$ values for $Fe(II)_{aq}$, $Fe(III)_{aq}$, and $Fe(OH)_3(s)$, as was done in the section on DIR above, as well as the approach outlined in the previous chapter for abiotic oxidation of $Fe(II)_{aq}$ (Chapter 10A; Beard and Johnson 2004). For example, if isotopic equilibrium is maintained between $Fe(II)_{aq}$ and $Fe(III)_{aq}$, the $\delta^{56}Fe$ value for the $Fe(III)_{aq}$ component is given by:

$$\delta_{Fe(III)aq} = \delta_{Fe(aq)\text{-}Total} + \Delta_{Fe(III)\text{ - }Fe(II)}\left(\frac{X_{Fe(II)}}{X_{Fe(II)} + X_{Fe(III)}}\right) \quad (20)$$

where $\delta_{Fe(aq)\text{-}Total}$ is the $\delta^{56}Fe$ value of the total aqueous Fe pool ($Fe(II)_{aq}$ and $Fe(III)_{aq}$), and $X_{Fe(II)}$ and $X_{Fe(III)}$ are the mole fractions of $Fe(II)_{aq}$ and $Fe(III)_{aq}$ in the total system, respectively. Note that if $X_{Fe(III)}$ is very small, which is the case for large k_2/k_1 ratios (Fig. 13), then $\delta_{Fe(aq)\text{-}Total}$ is essentially equal to the $\delta^{56}Fe$ value of $Fe(II)_{aq}$. Note also that the ratio $X_{Fe(II)}/(X_{Fe(II)} + X_{Fe(III)})$ will be unity at the beginning of the experiment (prior to oxidation), and will move to a constant value under steady-state conditions that is determined by the k_2/k_1 ratio.

At high k_2/k_1 ratios, the isotopic mass balance among the soluble (exchangeable) pools of Fe ($Fe(II)_{aq}$ and $Fe(III)_{aq}$) is essentially invariant with time. When $\delta_{Fe(aq)\text{-}Total} \approx \delta_{Fe(II)aq}$ and $X_{Fe(II)}/(X_{Fe(II)} + X_{Fe(III)}) \approx 1$, we may simplify Equation (20) to:

$$\delta_{Fe(III)aq} \approx \delta_{Fe(II)aq} + \Delta_{Fe(III)\text{-}Fe(II)} \quad (21)$$

Equation (21) is an excellent approximation to Equation (20) for moderate to high k_2/k_1 ratios (~10 and higher) for processes that occur by first-order kinetics. It is important to note, however, that a specific rate law does not appear anywhere in Equations (20) and (21), and they are equally valid for any reaction process where $X_{Fe(III)}$ is small. Equation (21) illustrates that oxidation of $Fe(II)_{aq}$ to $Fe(III)_{aq}$ produces a markedly different isotopic mass balance than that associated with DIR. In cases where the product of DIR is $Fe(II)_{aq}$, the concentration of this component is continually increasing, changing the relative mass balance among the exchangeable pools of Fe over time.

Next we explore using the $\delta^{56}Fe$ value of the ferric oxide/oxyhydroxide precipitate as a proxy for $\delta_{Fe(III)aq}$, which allows Equation (21) to be used to calculate the $\Delta_{Fe(III)\text{-}Fe(II)}$ fractionation from the measured $\delta^{56}Fe$ values for the ferric precipitate and $Fe(II)_{aq}$. This approach is valid when the molar proportion of $Fe(III)_{aq}$ is very small. However, if there is a significant Fe isotope fractionation between $Fe(III)_{aq}$ and ferric hydroxide precipitate, this must be taken into account. As discussed in the previous chapter (Chapter 10A; Beard and Johnson 2004), at low

$Fe(III)_{aq}/Fe(II)_{aq}$ ratios, and where isotopic equilibrium is maintained between $Fe(III)_{aq}$ and $Fe(II)_{aq}$, the effect of Fe isotope fractionation upon precipitation may be incorporated into the form of Equation (21) as:

$$\delta_{Fe(II)aq} - \delta_{FH} \approx \Delta_{Fe(III)\text{-}FH} - \Delta_{Fe(III)\text{-}Fe(II)} \quad (22)$$

where the $\delta^{56}Fe$ values for $Fe(II)_{aq}$ and the ferrihydrite precipitate are defined as $\delta_{Fe(II)aq}$ and δ_{FH}, respectively, and the Fe isotope fractionation between $Fe(III)_{aq}$ and ferrihydrite precipitate, and $Fe(III)_{aq}$ and $Fe(II)_{aq}$, is given by $\Delta_{Fe(III)\text{-}FH}$ and $\Delta_{Fe(III)\text{-}Fe(II)}$, respectively.

Croal et al. (2004) measured an approximate −1.5‰ fractionation between $Fe(II)_{aq}$ and ferrihydrite precipitate that formed during APIO. This fractionation is independent of the overall rate of oxidation, particularly if data early in the experiment are considered, when the measured isotopic differences between phases is least dependent upon a specific mechanistic model, such as closed-system equilibration or Rayleigh fractionation (Fig. 14). Precipitates that are removed early in the experiment are least likely to "back exchange" with the ambient aqueous Fe unless exchange rates are very rapid because they are not in contact with aqueous Fe for extended periods (Δ_2, Fig. 12). In interpreting these data, however, we are immediately faced with the ambiguity posed by Equation (22), which shows that in the absence of independent knowledge of the $\Delta_{Fe(III)\text{-}FH}$ fractionation, we cannot infer the Fe isotope fractionation produced during the oxidation step ($\Delta_{Fe(III)\text{-}Fe(II)}$). The Fe isotope fractionations measured by Croal et al. (2004), therefore, have several possible interpretations. First, the data may be interpreted to reflect Fe isotope fractionation between $Fe(II)_{aq}$ and $Fe(III)_{aq}$ of ~ −1.5‰, if $\Delta_{Fe(III)\text{ - }FH}$ is zero. In this case, the long residence time that is expected for $Fe(III)_{aq}$ (Fig. 13), relative to the time required to reach isotopic equilibrium between $Fe(II)_{aq}$ and $Fe(III)_{aq}$, suggests that the −1.5‰ $Fe(II)_{aq}$-$Fe(III)_{aq}$ fractionation would reflect an equilibrium

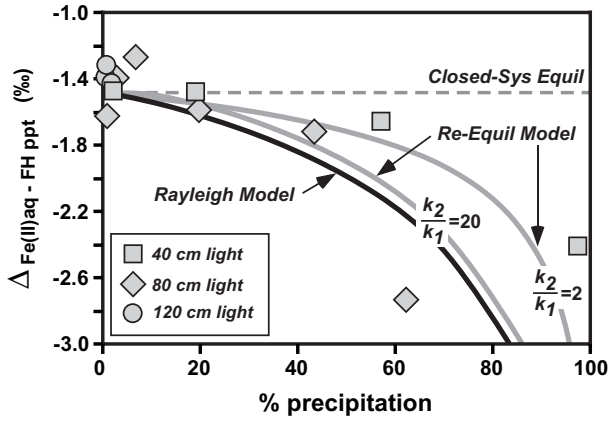

Figure 14. Measured Fe isotope fractionations between $Fe(II)_{aq}$ and ferrihydrite precipitates for the APIO experiments by Croal et al. (2004), relative to % total reaction (precipitation). A simple Rayleigh fractionation model is illustrated in the solid black curve, using a $\Delta_{Fe(II)aq\text{-}FH}$ fractionation of −1.5‰. Solid grey curves illustrate a two-step model, where the overall $Fe(II)_{aq}$–ferrihydrite fractionation proceeds first through a −2.9‰ equilibrium fractionation between $Fe(II)_{aq}$ and $Fe(III)_{aq}$, followed by a +1.4‰ between $Fe(III)_{aq}$ and ferrihydrite. Because the k_2/k_1 ratio in the first-order rate model affects the relative proportions of $Fe(II)_{aq}$ and $Fe(III)_{aq}$, the two-step model is a function of k_2/k_1 ratio; two examples are illustrated, one where the proportion of $Fe(III)_{aq}$ is relatively high ($k_2/k_1 = 2$), and one where the proportion of $Fe(III)_{aq}$ is relatively low ($k_2/k_1 = 20$). As the k_2/k_1 ratio increases beyond ~20 (very low proportion of $Fe(III)_{aq}$), the two-step model is well approximated by a single −1.5‰ fractionation between $Fe(II)_{aq}$ and ferrihydrite.

fractionation factor. This would be approximately half the −2.9‰ fractionation measured between Fe(II) and Fe(III) in dilute aqueous solutions (Johnson et al. 2002; Welch et al. 2003), and might suggest unique bonding environments for at least one Fe species during APIO as compared to $Fe(II)_{aq}$ and $Fe(III)_{aq}$ in abiologic systems.

The Fe(III)aq–ferrihydrite fractionation factor

The data of Croal et al. (2004) may also be interpreted to reflect a two-step process, where a −2.9‰ fractionation occurs between $Fe(II)_{aq}$ and $Fe(III)_{aq}$, accompanied by a +1.4‰ fractionation between $Fe(III)_{aq}$ and ferrihydrite upon precipitation, produces a net fractionation of −1.5‰. When cast in terms of common mechanistic models for separation of solid and liquid phases such as Rayleigh fractionation, it becomes clear that the two-step model produces essentially the same fractionation trend as a single −1.5‰ fractionation step between $Fe(II)_{aq}$ and ferrihydrite if the $Fe(III)_{aq}/Fe(II)_{aq}$ ratio is low (Fig. 14). As the $Fe(III)_{aq}/Fe(II)_{aq}$ ratio increases, however, the calculated net $Fe(II)_{aq}$-ferrihydrite fractionation in the two-step model deviates from that of simple Rayleigh fractionation (Fig. 14). Unfortunately, the scatter in the data reported by Croal et al. (2004), which likely reflects minor contamination of $Fe(II)_{aq}$ in the ferrihydrite precipitate, prevents distinguishing between these various models without consideration of additional factors.

A non-zero $\Delta_{Fe(III)\text{-}FH}$ fractionation might reflect kinetic or equilibrium isotope partitioning, and in the absence of independent measurements of the $\Delta_{Fe(III)\text{-}FH}$ fractionation factor under equilibrium conditions, as well as at different precipitation rates that are far from equilibrium, we must approach the problem indirectly. Equation (22) illustrates that the uncertainty in inferring the $\Delta_{Fe(III)\text{-}Fe(II)}$ fractionation is directly related to the uncertainty posed by the $\Delta_{Fe(III)\text{-}FH}$ fractionation factor when the proportion of $Fe(II)_{aq}$ is very small. The potential range of $\Delta_{Fe(III)\text{-}FH}$ under equilibrium and kinetic conditions may be explored through the experiments of Skulan et al. (2002), who investigated kinetic and equilibrium $[Fe^{III}(H_2O)_6]^{3+}$–hematite fractionations. There is some difficulty in comparing the experiments of Skulan et al. (2002) with those of Croal et al. (2004), because the ferric precipitates and temperatures were different. Skulan et al. (2002) observed that the kinetic $[Fe^{III}(H_2O)_6]^{3+}$–hematite fractionation, at 98°C, varied linearly with precipitation rate when precipitation rates were relatively low, on the order of 10^{-3} F/hour, where F is the fraction of the total precipitate. The largest kinetic $[Fe^{III}(H_2O)_6]^{3+}$ - hematite isotope fractionation observed by Skulan et al. (2002) was +1.3‰, where near-complete precipitation occurred over ~12 hours, equivalent to a relatively high rate of $\sim 10^{-1}$ F/hour. In contrast, Skulan et al. (2002) estimated that the equilibrium $[Fe^{III}(H_2O)_6]^{3+}$–hematite fractionation was near zero at 98°C, and it is possible, though unknown, that the equilibrium $[Fe^{III}(H_2O)_6]^{3+}$–ferrihydrite fractionation is similarly small at room temperature. If we assume that similar effects occurred during precipitation of ferrihydrite at the room temperature (~ 22°C) of the experiments by Croal et al. (2004), we would infer that moderately rapid ferrihydrite precipitation would produce significant kinetic $Fe(III)_{aq}$-ferrihydrite fractionations, but that slow precipitation of ferrihydrite may be associated with a $\Delta_{Fe(III)\text{-}FH}$ fractionation that is closer to zero.

We consider the relations between precipitation rate and the fractionation between $Fe(III)_{aq}$ and ferric oxide/hydroxide precipitates in Figure 15. The overall rates of Fe(II) oxidation and precipitation of ferrihydrite in the experiments by Croal et al. (2004) were several orders of magnitude lower than those studied by Skulan et al. (2002) where significant kinetic $[Fe^{III}(H_2O)_6]^{3+}$–hematite fractionations were observed, and this may suggest that the $\Delta_{Fe(III)\text{-}FH}$ fractionation was low in the experiments of Croal et al. (2004). Through variations in light intensity, the Fe(II) oxidation rates during APIO varied by nearly an order of magnitude (Fig. 15), and it is striking that the measured $Fe(II)_{aq}$–ferrihydrite fractionations were relatively constant, as determined for $Fe(II)_{aq}$–ferrihydrite pairs early in the experiment. This might suggest that kinetic isotope effects during precipitation were not important, provided the rate-

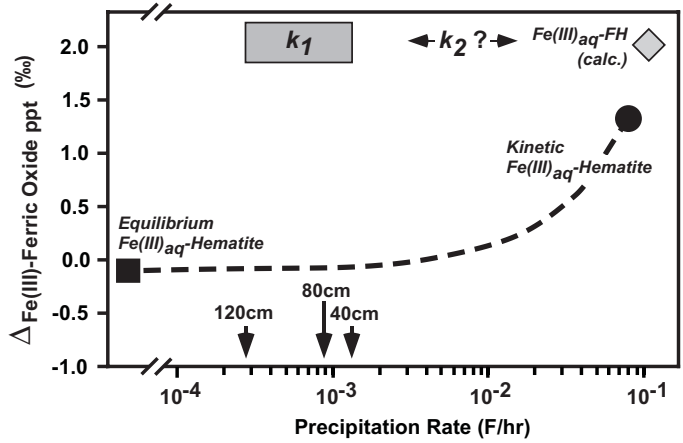

Figure 15. Illustration of possible variations in isotopic fractionation between $Fe(III)_{aq}$ and ferric oxide/hydroxide precipitate ($\Delta_{Fe(III)aq\text{-}Ferric\ ppt}$) and precipitation rate. Skulan et al. (2002) noted that the kinetic $\Delta_{Fe(III)aq\text{-}Ferric\ ppt}$ fractionation produced during precipitation of hematite from $Fe(III)_{aq}$ was linearly related to precipitation rate, which is shown in the dashed curve (precipitation rate plotted on log scale). The most rapid precipitation rate measured by Skulan et al. (2002) is shown in the black circle. The equilibrium $Fe(III)_{aq}$-hematite fractionation is near zero at 98°C, and this is plotted (black square) to the left of the break in scale for precipitation rate. Also shown for comparison is the calculated $Fe(III)_{aq}$-ferrihydrite fractionation from the experiments of Bullen et al. (2001) (grey diamond), as discussed in the previous chapter (Chapter 10A; Beard and Johnson 2004). The average oxidation-precipitation rates for the APIO experiments of Croal et al. (2004) are also noted, where the overall process is limited by the rate constant k_1. As discussed in the text, if the proportion of $Fe(III)_{aq}$ is small relative to total aqueous Fe, the rate constant for the precipitation of ferrihydrite from $Fe(III)_{aq}$ (k_2) will be higher, assuming first-order rate laws, although its value is unknown.

limiting step was varied in the experiments during changes in the overall oxidation rate, but this remains unknown in the experiments of Croal et al. (2004). The rate constant for precipitation of $Fe(III)_{aq}$ to ferrihydrite (k_2) is unknown, but is assumed to be significantly larger than k_1 in our first-order rate model. If the variations in light intensity varied only the rate constant for the oxidation step, k_1, and not, for example, the precipitation rate, k_2, then the range in overall oxidation rates place *no constraint* on inferring the value of the $\Delta_{Fe(III)\text{-}FH}$ fractionation based on the experimental observations of Skulan et al. (2002) (Fig. 15). Paradoxically, if k_2 is extremely high, as might be the case if the proportion of $Fe(III)_{aq}$ is quite low, very rapid precipitation of $Fe(III)_{aq}$ to ferrihydrite is unlikely to produce a significant $\Delta_{Fe(III)\text{-}FH}$ fractionation, as has been observed for very rapid (~1 s) oxidation of $Fe(II)_{aq}$ (Johnson et al. 2002).

Comparison with abiologic Fe(II) oxidation

The fractionation between $Fe(II)_{aq}$ and ferrihydrite of −1.5‰ measured during APIO by Croal et al. (2004) is somewhat similar to the −0.9‰ fractionation measured by Bullen et al. (2001) during abiotic oxidation of $Fe(II)_{aq}$ to ferrihydrite through reaction with an oxygenated solution. Bullen et al. (2001) interpreted this fractionation to reflect isotopic equilibrium between aqueous Fe(II) species, such as $[Fe^{II}(OH)(H_2O)_5]^+$ and $[Fe^{II}(H_2O)_6]^{2+}$, with the implicit assumption that there was no fractionation between aqueous Fe(II) and Fe(III), or upon precipitation of $Fe(III)_{aq}$ to ferrihydrite. As discussed in the previous chapter (Chapter 10A; Beard and Johnson 2004), the Bullen et al. (2001) model is unlikely, given the −2.9‰ equilibrium fractionation between $[Fe^{II}(H_2O)_6]^{2+}$ and $[Fe^{III}(H_2O)_6]^{3+}$ (Johnson et al. 2002; Welch et al. 2003), and the fact that isotopic exchange is so rapid between these species that

isotopic equilibrium will be maintained over the oxidation rates of the Bullen et al. (2001) experiment. Instead, these experiments likely reflect the combination of a −2.9‰ equilibrium fractionation between $[Fe^{II}(H_2O)_6]^{2+}$ and $[Fe^{III}(H_2O)_6]^{3+}$, and a +2.0‰ kinetic fractionation between $[Fe^{III}(H_2O)_6]^{3+}$ and ferrihydrite upon precipitation, although this later fractionation is inferred and has yet to be measured experimentally. The issue of the $\Delta_{Fe(III)\text{ - }FH}$ fractionation factor, under both equilibrium and kinetic conditions, once again becomes important. If the experiments by Bullen et al. (2001) in part reflect a +2.0‰ kinetic fractionation between $Fe(III)_{aq}$ and ferrihydrite, this is comparable to the kinetic $[Fe^{III}(H_2O)_6]^{3+}$–hematite fractionation measured by Skulan et al. (2002) when considered in terms of precipitation rates (Fig. 15), and the fact that the Bullen et al. (2001) experiments were run at lower temperatures.

If the rate constant for precipitation of $Fe(III)_{aq}$ to ferrihydrite (k_2) was $\geq 10^2$ times greater than the overall oxidation rate (k_1) during APIO, it is possible, based on the relations shown in Figure 15, that the $\Delta_{Fe(III)\text{-}FH}$ fractionation factor was +1 to +2‰, as noted in the "two-step" scenario above. If, however, k_2 was ~ ≤10 times greater than k_1, it is possible that the $\Delta_{Fe(III)\text{-}FH}$ fractionation factor was close to zero (Fig. 15). If the former case is correct, then we would infer that the isotopic fractionation between $Fe(II)_{aq}$ and $Fe(III)_{aq}$ during APIO is similar to that in dilute aqueous solutions. However, if the latter case is correct, the isotopic fractionation between soluble pools of $Fe(II)_{aq}$ and $Fe(III)_{aq}$ in the biologic system is unique relative to that in dilute aqueous solutions, perhaps indicating unique bonding environments caused by binding to biological ligands. If the $\Delta_{Fe(III)\text{-}FH}$ fractionation is zero in the biologic experiment, the relatively similar fractionations between $Fe(II)_{aq}$ and ferrihydrite in the experiments of Croal et al. (2004) and Bullen et al. (2001) are merely coincidental, reflecting the effects of kinetic fractionations during precipitation in the later study. Key resolutions to these issues include determining the $Fe(III)_{aq}$–ferrihydrite fractionation, as well as developing strategies to analyze the isotopic composition of the $Fe(III)_{aq}$ component directly, and these are important avenues for future research.

We wish to stress that comparison of the isotopic effects in biologic and abiologic systems will be most meaningful if experimental conditions are identical, where the only difference is the presence or absence of bacteria. The wide variety of buffers, growth media, and others conditions that are involved in biological experiments raise the possibility that spurious results may be obtained if these factors are not carefully controlled. Because speciation may exert a strong control on Fe isotope fractionations (Schauble et al. 2001), even small differences across experimental studies may be significant.

ISOTOPIC VARIATIONS PRODUCED DURING BIOGEOCHEMICAL CYCLING OF IRON

The kinetic and equilibrium Fe isotope fractionations associated with DIR and anaerobic APIO are summarized in Table 3. In this section, we use the Fe isotope fractionation factors determined for biologic systems to investigate the isotopic variations that may be produced during biogeochemical cycling of Fe. We discuss below two settings in which Fe cycling may occur. The first is redox cycling of Fe in a low-carbonate surface environment that involves oxidation of Fe(II) and reduction of Fe(III), such as might be found in a hydrothermal or hot spring pool. The second involves diagenetic reactions, with or without super-saturation of carbonate ion, where reductive dissolution of ferric oxide/hydroxide produces magnetite ± Fe carbonate.

Redox cycling of Fe by bacteria

Modern iron-depositing hot springs that are fed by Fe(II)-rich waters have been invoked as analogs to environments where active metal cycling most likely occurred in the

Precambrian (e.g., Pierson et al. 1999; Pierson and Parenteau 2000), which eventually may have been preserved as iron deposits (e.g., Wade et al. 1999). Oxidation of Fe(II) in the upper layers of microbial communities may occur abiotically through interaction of Fe(II) with an oxygenated atmosphere, or through biologic activity. For example, Fe(II) may be oxidized through locally increased oxygen contents generated by cyanobacteria in the upper photic region of a microbial community. Alternatively, phototrophic Fe(II) oxidation may occur in the absence of oxygen by purple and green bacteria, and this is illustrated in Figure 16. Finally, reductive dissolution of ferric oxide/hydroxide precipitates may occur at the sediment-water interface at the bottom of hot springs by DIR (Fig. 16), completing the Fe redox cycle (e.g., Nealson and Stahl 1997). To illustrate the isotopic variations that may be produced in such a model, we define the following fluxes:

$$J_{\text{Fe(II)-Ext}} = J_{2\text{IE}} \tag{23}$$

the external flux of Fe(II) into the system;

$$J_{\text{Fe(III)-ppt}} = J_{3\text{O}} \tag{24}$$

the flux of Fe precipitated from the Fe(II) pool as ferric oxyhydroxides, produced by Fe(II)-oxidizing bacteria;

$$J_{\text{Fe(II)-Bio}} = J_{2\text{IB}} \tag{25}$$

the flux of Fe returned to the main pool as Fe(II), generated by Fe(III)-reducing bacteria.

We further constrain the system to have no Fe loss. In addition, we define the following:

$$\Delta_{32} = \delta^{56}\text{Fe}_{\text{Ferric Oxide ppt}} - \delta^{56}\text{Fe}_{\text{Fe(II)}} = +1.5‰ \tag{26}$$

which is the Fe isotope fractionation factor between ferric oxide/hydroxide precipitate and Fe(II) in the pool, produced by Fe(II)-oxidizing bacteria.

We define the δ^{56}Fe of the Fe(II) that is input into the pool at any time as:

$$\delta^{56}\text{Fe}_{2\text{I}} = \delta^{56}\text{Fe}_{2\text{IE}}\left(\frac{J_{2\text{IE}}}{J_{2\text{IE}} + J_{2\text{IB}}}\right) + \delta^{56}\text{Fe}_{2\text{IB}}\left(\frac{J_{2\text{IB}}}{J_{2\text{IE}} + J_{2\text{IB}}}\right) \tag{27}$$

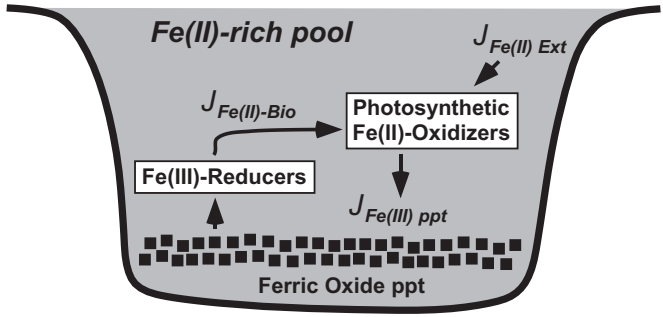

Figure 16. Conceptual model for biological redox cycling in a hot spring environment. Influx of external aqueous Fe(II) [$J_{\text{Fe(II)-Ext}}$] may reflect hydrothermal fluids or other sources of $\text{Fe(II)}_{\text{aq}}$. Oxidation of $\text{Fe(II)}_{\text{aq}}$ is envisioned to occur by Fe(II)-oxidizing phototrophs in anaerobic conditions, but could also occur through interaction of $\text{Fe(II)}_{\text{aq}}$ with an oxygen-rich atmosphere. Oxidation of Fe(II) produces a flux of ferric oxide/hydroxide precipitates [$J_{\text{Fe(III) ppt}}$] that settle to the lower, anaerobic sections of the pool. These ferric precipitates are in turn partially reduced by DIR bacteria, returning a flux of $\text{Fe(II)}_{\text{aq}}$ to the pool [$J_{\text{Fe(II)-Bio}}$].

Following the mass-flux equations developed for open-system magma chambers by DePaolo (1981), we will define a flux ratio of Fe(II) into the pool relative to Fe(III) out of the pool as:

$$r = \frac{J_{2I}}{J_{3O}} = \frac{J_{2IE} + J_{2IB}}{J_{3O}} \tag{28}$$

We will restrict r to values less than unity, which is necessary to accumulate an Fe deposit. Solution of the time derivatives, expressed as F (fraction of liquid remaining in the pool), following the approach of DePaolo (1981), but cast in terms of fluxes, produces:

$$\delta^{56}Fe_{POOL} = \delta^{56}Fe^{I}_{POOL} + \left(1 - F^{[-r/(r-1)]}\right)\left(\delta^{56}Fe_{2I} - \frac{\Delta_{32} + r\delta^{56}Fe^{I}_{POOL}}{r}\right) \tag{29}$$

where $\delta^{56}Fe^{I}_{POOL}$ is the initial $\delta^{56}Fe$ value of the pool (set equal to $\delta^{56}Fe_{2IE}$).

An end-member case would be precipitation of ferric oxyhydroxide by photosynthetic Fe(II)-oxidizing bacteria through simple Rayleigh fractionation, with no external Fe(II) flux or return of Fe(II) to the pool from Fe(III)-reducing bacterial activity, which will produce extreme Fe isotope compositions, but only in the latest fluids and precipitates (Fig. 17). In

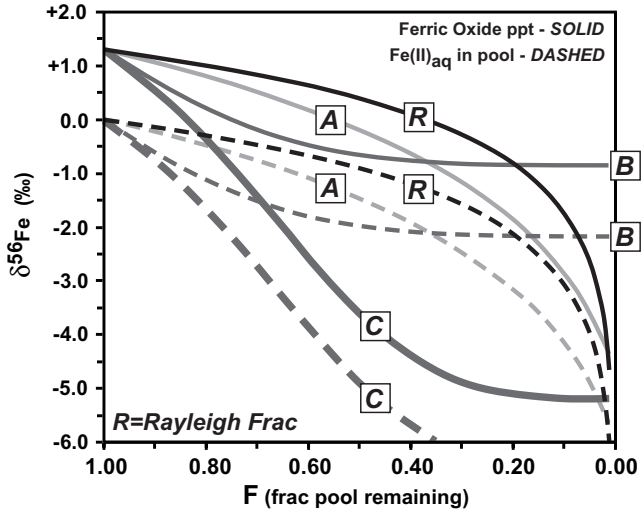

	IN Fluxes		OUT Flux
	$J_{Fe(II)\text{-}Ext}$	$J_{Fe(II)\text{-}Bio}$	$J_{Fe(III)\ ppt}$
Case A	*1*	*1*	*5*
Case B	*3*	*1*	*5*
Case C	*1*	*3*	*5*

Figure 17. Predicted Fe isotope variations produced by redox cycling of Fe due to APIO and DIR by bacteria, as envisioned from Fig. 16. The initial $\delta^{56}Fe$ of the pool, as well as that of the influx of $Fe(II)_{aq}$ [$J_{Fe(II)\text{-}Ext}$] is assumed to be zero. Solid lines show the $\delta^{56}Fe$ values for ferric oxide/oxyhydroxide deposits as a function of solidification of the pool as an iron deposit is formed, and dashed lines show the $\delta^{56}Fe$ values for $Fe(II)_{aq}$. Depending upon the relative fluxes of external $Fe(II)_{aq}$ [$J_{Fe(II)\text{-}Ext}$], return of Fe(II) to the pool by DIR [$J_{Fe(II)\text{-}Bio}$], and precipitation of ferric oxide/oxyhydroxides by APIO [$J_{Fe(III)\ ppt}$], a wide range of $\delta^{56}Fe$ values can be produced.

the case of a modest return of Fe(II) to the pool from Fe(III)-reducing bacteria, as well as a continued modest influx of external Fe(II) (J_{2E}:J_{2B}:J_{3O} of 1:1:5), the δ^{56}Fe values of the pool and ferric oxide/hydroxide precipitates decrease slightly more rapidly than in the Rayleigh model. In the case where there is a very high flux of external Fe(II) into the pool (J_{2E}:J_{2B}:J_{3O} of 3:1:5), the δ^{56}Fe values of the pool and the resulting ferric oxide deposit initially drop, but then level off to a pseudo steady-state condition after about 40% of the pool has been solidified.

The most dramatic shifts in Fe isotope compositions are predicted for cases where there is a large return of Fe(II) from DIR bacterial activity, but small external Fe(II) flux (i.e., J_{2E}:J_{2B}:J_{3O} of 1:3:5), where, after ~40–50% solidification of the pool, δ^{56}Fe values of the ferric oxyhydroxide precipitate will drop 4–5‰. The calculations in Figure 17 illustrate that a wide range in Fe isotope compositions may be expected in the relatively simple system $Fe(II)_{aq}$-$Fe(III)_{aq}$-ferric oxide/hydroxide if extensive re-processing of Fe occurs, despite the fact that the Fe isotope fractionation factor used in the model is very similar for APIO and DIR (Table 3). Experimental verification of the predicted variations in δ^{56}Fe values during biological redox cycling of Fe in a system of Fe(II)-oxidizing and Fe(III)-reducing bacteria would be useful in predicting Fe isotope fractionations expected for modern or ancient microbial communities.

The large range in δ^{56}Fe values that are predicted for a ferric oxide/hydroxide deposit from the above model reflects incomplete reduction of ferric oxide/hydroxide precipitates by DIR bacteria. Although experimental studies of DIR using poorly crystalline HFO and rich growth media commonly run to completion, such conditions may be unrepresentative of natural conditions (e.g., Glasauer et al. 2003). Natural environments will generally involve more crystalline ferric oxide/hydroxide minerals and be poorer in nutrients, resulting in incomplete dissolution by DIR bacteria. In contrast, natural Fe(III)-bearing clay minerals may have very high surface areas, and, in fact, may be equally reactive as poorly crystalline ferric hydroxides (e.g., Kostka et al. 1999a). An important, yet largely unexplored, component to preservation of the large range in δ^{56}Fe values predicted in Figure 17 is the degree of isotopic exchange between oxide/hydroxide precipitates and aqueous Fe, which will be an important factor in determining the extent to which the predicted Fe isotope variations will be preserved in the rock record. Initial results investigating isotopic exchange between $Fe(III)_{aq}$ and ferrihydrite suggest that exchange is limited to surface Fe atoms (Poulson et al. 2003); for all but the smallest ferric hydroxide particles, these results suggest that little "back exchange" occurs between aqueous Fe and solid ferric hydroxide.

Isotopic variations in marine settings

The occurrence of isotopic and morphologic evidence for bacterial activity in marine sedimentary rocks makes such sequences a logical target for Fe isotope studies as a tracer for bacterial metabolism. One of the largest repositories of Fe that was sequestered from the oceans lies in Archean and Proterozoic Banded Iron Formations (BIFs). The ultimate source of Fe in BIFs is generally thought to be Mid-Ocean Ridge (MOR) hydrothermal fluids, based largely on REE and Nd isotope data and the assumption that REE and Fe sources would be similar (e.g., Klein and Beukes 1989; Beukes and Klein 1990; Bau and Dulski 1996). Possible relations between BIF formation and biologic activity have been discussed for many decades (e.g., Harder 1919; Barghoorn 1981; Baur et al. 1985; LaBerge et al. 1987; Nealson and Myers 1990; Schopf 1992; Skinner 1993; Aisen 1994; Brown et al. 1995; Konhauser et al. 2002). Iron isotope fractionations produced during APIO and DIR may be used to evaluate the role bacteria may have played in BIF genesis.

Many exposed BIF sequences have been subjected to deep weathering and metamorphism, where hematite and goethite are, for the most part, secondary alteration products (e.g., Beukes and Klein 1992). In a few cases, however, primary hematite is found as finely disseminated

grains in carbonate- and chert-facies BIFs from fresh drill cores (e.g., Beukes et al. 1990). The δ^{56}Fe values of primary hematite from the Kuruman Iron Formation in South Africa varies from −0.7 to +0.8‰ (Johnson et al. 2003), which is significantly more variable than the near-zero values expected for ferric oxide/hydroxides derived from terrestrial weathering processes (Chapter 10A; Beard and Johnson 2004). The δ^{56}Fe values measured for primary hematite in BIFs may be explained through complete oxidation of MOR $Fe(II)_{aq}$ hydrothermal sources ($\delta^{56}Fe < 0$), incomplete oxidation of $Fe(II)_{aq}$ during anaerobic photosynthesis ($\delta^{56}Fe>0$), or might reflect incomplete abiotic oxidation if atmospheric oxygen contents were high ($\delta^{56}Fe>0$) (Fig. 18) (Johnson et al. 2003; Croal et al. 2004). As noted by Croal et al. (2004), distinction between abiotic oxidation and anaerobic photosynthetic oxidation may not be possible based on Fe isotope compositions alone and likely requires independent knowledge of ambient atmospheric oxygen contents.

Although the majority of attention in discussions on the origins of BIFs has been on the oxide facies, siderite facies rocks are equally important in many BIF sequences. Reaction of $Fe(II)_{aq}$ and dissolved carbonate with hematite to form siderite and magnetite has been hypothesized to be an important diagenetic process in marine basins during formation of some BIFs if sulfate contents were low (e.g., Klein and Beukes 1989; Beukes et al. 1990; Kaufman 1996; Sumner 1997). In Figure 18 we assume that $Fe(II)_{aq}$ was derived either from MOR sources or DIR, or a combination of the two, which reacted with ferric oxide precipitates to form magnetite or dissolved carbonate to produce siderite.

Under oxic conditions, primary ferric oxides derived from weathering will have δ^{56}Fe values near zero (Chapter 10A; Beard and Johnson 2004), and we will assume this isotope composition for simplicity. If the majority of $Fe(II)_{aq}$ was derived through DIR, the δ^{56}Fe value of $Fe(II)_{aq}$ is taken as ~ −1.3‰ (Beard et al. 1999, 2003a), assuming equilibrium conditions; lower δ^{56}Fe values would be expected if kinetic conditions prevailed (Johnson et al. 2004a). In the case where the $Fe(II)_{aq}$ reservoir is largely produced by DIR, and when there is excess $Fe(II)_{aq}$, the δ^{56}Fe values for magnetite, siderite, and "ankerite" would be approximately 0.0, −1.3, and −2.2‰, respectively, using the equilibrium Fe isotope fractionation factors summarized in Table 3 (Fig. 18). If $Fe(II)_{aq}$ sources were dominated by hydrothermal fluids that were associated with MOR activity, and we assume this source had a δ^{56}Fe value of ~ −0.5‰ as measured today (Sharma et al. 2001; Beard et al. 2003b), the predicted δ^{56}Fe values for magnetite, siderite, and "ankerite" would be slightly higher, at ~ +0.8, −0.5, and −1.4‰, respectively (Fig. 18), again assuming excess $Fe(II)_{aq}$. These ranges in δ^{56}Fe values for magnetite, siderite, and ankerite indeed span those measured in BIFs (Johnson et al. 2003). If ambient $Fe(II)_{aq}$ contents were low, and diagenetic reactions ran to completion, the final δ^{56}Fe values for magnetite and Fe carbonates will reflect the relative proportions of Fe sources, and will likely lie much closer to the δ^{56}Fe values of primary ferric oxide/hydroxides. That the δ^{56}Fe values for the Fe(II)-bearing minerals in BIFs do not lie near zero suggests that they formed in the presence of substantial quantities of $Fe(II)_{aq}$, and do not simply reflect "closed-system" redox processing that ran to completion.

The wide range in δ^{56}Fe values for magnetite relative to those of siderite that are observed in BIFs may reflect mixing between two different sources of Fe (Johnson et al. 2004a). Based on the isotopic fractionations listed in Table 3, magnetite that has the highest δ^{56}Fe values, and accompanying large $\Delta_{Magnetite\text{-}Siderite}$ fractionations between adjacent bands, appears to be well explained by $Fe(II)_{aq}$ sources derived from MOR hydrothermal sources (Fig. 19), assuming a $\Delta_{Fe(II)\text{-}Magnetite}$ fractionation of −1.3‰. Assuming that the δ^{56}Fe value for MOR sources of $Fe(II)_{aq}$ was the same during formation of BIFs in the late Archean to early Proterozoic as it is today, magnetite that has moderate to low δ^{56}Fe values, from near zero to negative values, seems to require different sources for $Fe(II)_{aq}$. Johnson et al. (2004a) argued that the source for very low δ^{56}Fe values was mostly likely $Fe(II)_{aq}$ which was produced by DIR of ferric oxides (Fig. 19).

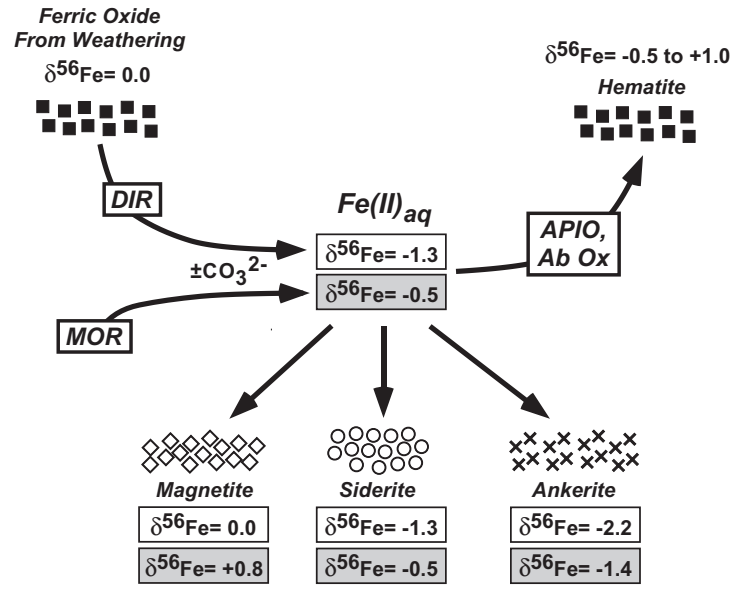

Figure 18. Possible Fe isotope compositions that may be produced by diagenetic reactions associated with DIR of ferric oxide/oxyhydroxide sediments, where $Fe(II)_{aq}$ reacts with hematite/goethite/ferrihydrite to produce magnetite, or, in the presence of carbonate ion ± Ca, siderite and ankerite. Such reactions may be envisioned to be characteristic of those that occur in relatively anoxic marine basins. $Fe(II)_{aq}$-magnetite, $Fe(II)_{aq}$-siderite, and $Fe(II)_{aq}$-ankerite isotope fractionation factors pertinent to biologic systems are from Table 3. $\delta^{56}Fe$ values in the non-shaded boxes assume that $Fe(II)_{aq}$ is dominated by DIR, where the ferric oxide (electron acceptor) has a $\delta^{56}Fe$ value of zero. $\delta^{56}Fe$ values in the shaded boxes assume that the isotopic composition of $Fe(II)_{aq}$ is dominated by Mid-Ocean Ridge (MOR) hydrothermal sources (Sharma et al. 2001; Beard et al. 2003b); this does not rule out a biologic input, but emphasizes an "external" (MOR) control of the $\delta^{56}Fe$ value for $Fe(II)_{aq}$. Oxidation of $Fe(II)_{aq}$ generated by DIR or MOR sources produces ferric oxides that have slightly negative to positive $\delta^{56}Fe$ values (upper left), dependent upon the sources of Fe(II). Oxidation may occur by APIO or by abiotic processes (Ab Ox); fractionation factors from Table 3.

Magnetite that has $\delta^{56}Fe$ values near zero might reflect formation during slow (equilibrium) reduction rates, whereas the lowest $\delta^{56}Fe$ values might reflect rapid Fe(III) reduction and kinetic isotope fractionation (Fig. 19), or multiple reduction cycles. The correlation between $\Delta_{Magnetite\text{-}Siderite}$ and $\delta^{56}Fe$ of magnetite observed in BIFs therefore probably reflects changes in the $\delta^{56}Fe$ values of aqueous Fe(II) involved in magnetite formation, reflecting a spectrum between abiotic MOR sources and biologic sources (Fig. 19). Based on the data at hand, magnetite that has negative $\delta^{56}Fe$ values appears to be an Fe isotope fingerprint for biological processing of Fe that is recorded in the ancient rock record.

The contrast in $\delta^{56}Fe$ values for Fe carbonates and magnetite from adjacent bands in BIFs can be explained through formation from a common fluid in cases where the $\delta^{56}Fe$ value of magnetite is positive; in these cases, the major source for $Fe(II)_{aq}$ for both siderite and magnetite appears to be MOR hydrothermal sources. For magnetite that has $\delta^{56}Fe$ values $\leq 0‰$, however, layers of adjacent magnetite and siderite would not to be in isotopic equilibrium, where magnetite appears to be related to DIR. The relatively constant $\delta^{56}Fe$ values for siderite from BIFs studied to date suggests that most precipitated from MOR sources of $Fe(II)_{aq}$. Although DIR may produce siderite, the Fe isotope data obtained on siderite-facies BIFs so far suggests that DIR bacteria were not involved. A possible explanation would be that

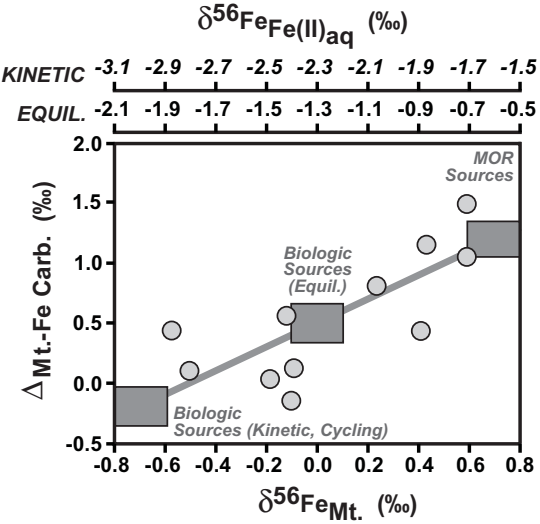

Figure 19. Iron isotope fractionations between magnetite and Fe carbonates from adjacent bands in Banded Iron Formations (Johnson et al. 2004a), compared to $Fe(II)_{aq}$ sources and Fe pathways inferred from the Fe isotope fractionations given in Table 3. $\delta^{56}Fe_{Mt}$ values are as measured, and the scales for $\delta^{56}Fe_{Fe(II)aq}$ values (top) are based on the equilibrium $\Delta_{Fe(II)aq\text{-}Magnetite}$ fractionation of −1.3‰, or −2.3‰ for kinetic fractionations (Table 3). These results suggest that magnetite which has moderately positive $\delta^{56}Fe$ values probably formed in equilibrium with MOR hydrothermal sources for $Fe(II)_{aq}$. In contrast, the lower inferred $\delta^{56}Fe$ values for $Fe(II)_{aq}$ for magnetite that has $\delta^{56}Fe \leq 0$‰ would apparently require production of $Fe(II)_{aq}$ through DIR, using the fractionation factors determined by Johnson et al. (2004a), where the lowest values would be expected to have the largest contribution from kinetic isotope fractionation, or reflect biologic cycling of Fe. The solid line is a mixing line based on changing $\delta^{56}Fe$ values for $Fe(II)_{aq}$, a constant $\Delta_{Fe(II)aq\text{-}Magnetite}$ fractionation of −1.3‰, and a constant $\delta^{56}Fe$ value for siderite of −0.5‰ (the average of that in BIFs; Johnson et al. 2003). The model assumes that isotopic equilibrium is maintained between $Fe(II)_{aq}$ and magnetite, but not between adjacent siderite and magnetite bands. Regression of the measured $\Delta_{Magnetite\text{-}Siderite}$–$\delta^{56}Fe_{Mt}$ relations produces a slope that is identical to that of the illustrated mixing line, suggesting that the measured variations reflects precipitation of magnetite from variable sources of $Fe(II)_{aq}$, scattering between an MOR (high $\delta^{56}Fe$) and a biogenic (low $\delta^{56}Fe$) component. Adapted from Johnson et al. (2004a).

precipitation of ferric oxides/hydroxides in the upper water column was minimal during times of siderite formation, which would depress DIR activity.

Identification of significant masses of magnetite-rich BIF layers that formed in equilibrium with a low-$\delta^{56}Fe$, Fe(II)-rich fluid would have important implications for the sizes of various aqueous Fe reservoirs in the oceans if they were relatively anoxic. The long residence time of Fe in an anoxic water mass would make it resistant to changes in $\delta^{56}Fe$ values (Johnson et al. 2003) from, for example, a MOR hydrothermal source ($\delta^{56}Fe \geq -0.5$‰) to one dominated by DIR ($\delta^{56}Fe \leq -1.3$‰). If the low $\delta^{56}Fe$ values for $Fe(II)_{aq}$ inferred from the low-$\delta^{56}Fe$ magnetite in BIFs (Fig. 19) reflect those of the open ocean, the biomass required to overwhelm the MOR sources must have been tremendous. Such a scenario, however, is inconsistent with the relative homogeneity in $\delta^{56}Fe$ values for interbedded siderite-rich layers in BIFs. Large changes in $\delta^{56}Fe$ values for ambient $Fe(II)_{aq}$ over the timescales involved in deposition of alternating cm-thick magnetite- and siderite-rich layers is very unlikely if the residence time of Fe was long. Instead, the most plausible explanation may be that the $\delta^{56}Fe$ values for siderite-rich layers do indeed reflect those of the open ocean water masses, dominated by a

MOR hydrothermal component, but that the very low δ^{56}Fe values inferred for $Fe(II)_{aq}$ from low δ^{56}Fe magnetite reflect interstitial pore waters and/or bottom waters that were closely associated with DIR bacteria, and not those of the open oceans. A substantial biomass of DIR bacteria is still required to process the very large inventory of Fe that is sequestered in BIFs as low-δ^{56}Fe magnetite, although not so extensive as that which would be required to lower the δ^{56}Fe values of the open oceans if the oceans were rich in $Fe(II)_{aq}$.

CONCLUSIONS

A significant proportion of the Fe isotope literature has focused on use of Fe isotopes as a "biosignature" for life, and the mechanisms by which Fe isotope variations may be produced in biologic systems has been the focus of this chapter. At first glance, an Fe isotope biosignature would seem to require isotopic fractionations that can only be produced by biology, which a substantial body of data clearly show is not the case. Although there is no question that metabolic processing of Fe produces isotopic fractionation (Beard et al. 1999, 2003a; Croal et al. 2004; Johnson et al. 2004a), it is also true that similar Fe isotope fractionations may be produced by abiologic processes (Anbar et al. 2000; Bullen et al. 2001; Johnson et al. 2002; Roe et al. 2003; Welch et al. 2003; Icopini et al. 2004). A rapidly growing set of experimental studies in abiologic and biologic systems allows us to place some constraints on the issue, and identify future directions of research that are needed.

Experimental studies of abiologic Fe isotope fractionation that seem most applicable to natural systems include fractionations between $Fe(III)_{aq}$ and $Fe(II)_{aq}$, $[Fe^{III}(H_2O)_6]^{3+}$–hematite, $[Fe^{II}(H_2O)_6]^{2+}$–siderite, oxidation of $Fe(II)_{aq}$ to ferrihydrite, and sorption of Fe(II) to ferric hydroxides (Table 3). Additional studies such as those involving concentrated HCl solutions and ion-exchange chromatography (e.g., Anbar et al. 2000; Matthews et al. 2001; Roe et al. 2003), while providing insight into the effects of different bonding environments, have less applicability to natural systems. For example, the octahedral Fe(III) chloro complexes are expected to be lower in $^{56}Fe/^{54}Fe$ ratios by 5 to 10‰ as compared to the hexaquo Fe(III) complex at room temperature (Schauble et al. 2001; Anbar et al. 2004), highlighting the fact that the isotopic compositions of very acidic, high-Cl^- fluids which essentially only exist in the laboratory will be markedly different than those found in virtually all natural environments that may support life.

The equilibrium isotopic fractionation between $[Fe^{III}(H_2O)_6]^{3+}$ and $[Fe^{II}(H_2O)_6]^{2+}$ of +2.9‰ at room temperature (Table 3), which appears to be constant over a range of Cl^- contents, provides a benchmark with which to compare isotopic fractionations during redox cycling of Fe. Although the measured isotopic contrast between ferric oxide/hydroxide substrate and $Fe(II)_{aq}$ during DIR is approximately half that measured between $Fe(III)_{aq}$ and $Fe(II)_{aq}$ (Table 3), the uncertainty in calculating the isotopic compositions of the soluble Fe(III) component based on mass-balance modeling discussed in this chapter makes it difficult at present to compare the isotopic fractionations observed during DIR with an "equivalent" abiologic system. There is little doubt that many DIR bacteria are capable of producing soluble reservoirs of Fe(III), but this component has yet to be analyzed directly so that it may be compared to the isotopic compositions of $Fe(II)_{aq}$ that is produced. An important goal for future work will be isolation of the soluble Fe(III) component, identification of the ligands that are bound to it, and direct isotopic analysis.

The observation that DIR produces $Fe(II)_{aq}$ that has low δ^{56}Fe values might be taken as a biosignature for this type of Fe metabolism. Complicating factors, however, include the effects of intermediate Fe(II) species, including sorbed Fe(II) and poorly defined NMNC Fe(II) solids. Although the evidence at hand suggests that the effects of these intermediate species in determining the δ^{56}Fe values for $Fe(II)_{aq}$ are significant during rapid Fe(III) reduction rates

when kinetic effects are most likely, these issues require further study before we may fully understand their role in determining the Fe isotope fractionations that are produced by DIR in natural systems. Because the rates of Fe(III) reduction are expected to be generally far slower in nature than in most experiments, due, for example, to the greater crystallinity of ferric oxide/hydroxides and limited nutrients in natural systems, it seems likely that Fe isotope fractionations will tend to reflect equilibrium conditions in nature. As such, the low δ^{56}Fe values for $Fe(II)_{aq}$ that have been determined in experiments that involve very slow rates of DIR using crystalline substrates seem to be the most analogous to those expected in natural systems. An important, though completely unexplored avenue of research, is DIR involving Fe(III)-bearing clay minerals.

For mineral end products of DIR that are most likely to be preserved in the rock record, such as siderite and magnetite, if their δ^{56}Fe values are low, this may reflect precipitation from Fe(II)-bearing fluids that have the low-δ^{56}Fe fingerprint of DIR. It is not yet clear if the small (~0.5‰) difference in the $Fe(II)_{aq}$-siderite fractionation factor in abiologic and biologic experiments (Table 3) is significant, but their gross similarity suggests that siderite which has low δ^{56}Fe values probably precipitated from Fe(II)-bearing fluids of equal or slightly higher $^{56}Fe/^{54}Fe$ ratios; such low δ^{56}Fe values would appear to be best explained by DIR. A critical issue, however, remains the isotopic effect of cation substitution, which commonly occurs in natural Fe carbonates and may substantially affect the fluid-mineral Fe isotope fractionation factors. The case for a DIR fingerprint in low-δ^{56}Fe magnetite appears stronger, where the $^{56}Fe/^{54}Fe$ ratios for $Fe(II)_{aq}$ in equilibrium with magnetite would be ~ 1.3‰ lower, again consistent with $Fe(II)_{aq}$ that was produced by DIR.

The confidence with which $Fe(II)_{aq}$ that has δ^{56}Fe values ≤ -1.3‰ is a biosignature for DIR may be evaluated through abiotic reductive dissolution experiments of ferric oxide/hydroxides (e.g., Cornell and Schwertmann 1996; Larsen and Postma 2001), which has not yet been pursued in terms of possible Fe isotope fractionations. Could it be that the mixed Fe(III)-Fe(II) surface complexes that are likely to be present during abiotic reduction of ferrihydrite, goethite, or hematite (e.g., Hering and Stumm 1990) may produce an apparent Fe isotope fractionation between $Fe(II)_{aq}$ and ferric substrate that is similar to that observed during DIR? Although rapid sorption of Fe(II) to ferric oxide/hydroxide substrates produces low δ^{56}Fe values for the remaining aqueous Fe(II), the isotopic effects under equilibrium conditions are inferred to be less extreme. It is possible, however, that sorbed Fe(III) may have relatively high δ^{56}Fe values, even under equilibrium conditions, and this is a potential means to produce $Fe(II)_{aq}$ that has low δ^{56}Fe values. As demonstrated by the mass-balance calculations discussed in this chapter, a sorbed ≡[Fe(II), Fe(III)] phase would have to form a significant proportion of the exchangeable pool of Fe for it to influence the Fe isotope compositions of $Fe(II)_{aq}$. Such detailed experimental studies, including assessment of isotopic mass balance and exchange kinetics, have only just begun.

APIO produces ferric hydroxide precipitates that have relatively high δ^{56}Fe values, but similar effects may be observed during moderately rapid abiotic oxidation of $Fe(II)_{aq}$. Although the pathways involved in APIO are less complicated than those associated with DIR, direct measurement of intermediate species such as soluble or $Fe(III)_{aq}$ has not been done, raising the possibility that isotopic fractionation between $Fe(III)_{aq}$ and ferric hydroxide may be a significant contribution to the overall measured fractionation. The problem may be addressed through experiments aimed at determining the $Fe(III)_{aq}$-ferric hydroxide fractionation factor under equilibrium and kinetic conditions, including a range of precipitation rates. It is therefore unclear at present if ferric oxides that have positive δ^{56}Fe values in the rock record reflect APIO or abiotic oxidation of $Fe(II)_{aq}$ by high oxygen contents, or, perhaps, UV photo-oxidation. In addition, only one of the pathways in which Fe(II) is oxidized by biological processing has been explored in experiments, and experimental studies of other oxidative pathways such as chemolithotrophic oxidation or nitrate reduction would be valuable.

A useful thought experiment might be to pose the question that if abiotic reductive dissolution of ferric oxides/hydroxides and abiotic oxidation of Fe(II) to ferric oxide/hydroxide precipitates are eventually shown to produce similar overall Fe isotope fractionations as DIR and APIO, respectively, would Fe isotopes be useful as a biosignature at all? We do not know if the preceding hypothesis is correct, of course, but the implications of such a question bear on future directions Fe isotope geochemistry may take. If redox cycling of Fe involves ferric oxides/hydroxides, a mechanism for oxidation of the primary "lithologic" sources of Fe(II) is required. In the absence of UV photo-oxidation as a major process for oxidizing Fe, we are left with APIO, or increases in ambient O_2 contents due to photosynthesis where H_2O is the electron donor; either of these later cases would indicate that Fe isotopes either directly or indirectly indicate the presence of life, although the isotopic compositions may not distinguish between possible metabolic processes. Assuming a mechanism for producing ferric Fe oxides/hydroxides, reduction in the absence of biology would seem to require a redox-stratified environment, where, for example, $Fe(II)_{aq}$ in anaerobic environments reacted with ferric oxide/hydroxides that formed under oxidizing conditions. One possibility for production of reducing environments is through sulfide emanation from MOR vents, but the very low solubility of sulfide minerals suggests that large quantities of $Fe(II)_{aq}$ are unlikely to exist in sulfide-rich environments (e.g., Canfield et al. 1992). It may be that formation of redox stratifications on a planetary body, which should produce significant Fe isotope fractionations, are most likely to be produced by life. In summary, evaluation of the usefulness of Fe isotopes in tracing biological processing requires detailed consideration of the processes and environments in which biological cycling of Fe is likely to occur. Simple comparisons of the range in Fe isotope compositions produced by biological and abiological processes (e.g., Rouxel et al. 2003, 2004) may have limited usefulness in this regard.

A clear avenue of future research is to explore the S-Fe redox couple in biologic systems. Bacterial sulfate reduction and DIR may be spatially decoupled, dependent upon the distribution of poorly crystalline ferric hydroxides and sulfate (e.g., Canfield et al. 1993; Thamdrup and Canfield 1996), or may be closely associated in low-sulfate environments. Production of H_2S from bacterial sulfate reduction may quickly react with $Fe(II)_{aq}$ to form iron sulfides (e.g., Sørensen and Jeørgensen 1987; Thamdrup et al. 1994). In addition to these reactions, Fe(III) reduction may be coupled to oxidation of reduced S (e.g., Thamdrup and Canfield 1996), where the net result is that S and Fe may be cycled extensively before they find themselves in the inventory of sedimentary rocks (e.g., Canfield et al. 1993). Investigation of both S and Fe isotope fractionations produced during biochemical cycling of these elements will be an important future avenue of research that will bear on our understanding of the isotopic variations of these elements in both modern and ancient environments.

ACKNOWLEDGMENTS

Reviews by Francis Albarède, Ariel Anbar, and Susan Glasauer are appreciated. Sue Brantley is thanked for sharing several preprints and for additional comments on the paper. We also thank the Fe isotope group at UW Madison for their discussions and comments on drafts of the manuscript. Financial support for the research embodied here was provided by NASA, NSF, the Packard Foundation, and the University of Wisconsin. In particular, the NASA Astrobiology Institute supported a large portion of our work on Fe isotope fractionations in biologic systems. Collaborations with Carmen Agular, Nic Beukes, Paul Braterman, Lea Cox, Laura Croal, Andreas Kappler, Kase Klein, Hiroshi Ohmoto, Rebecca Poulson, Silke Severmann, Joseph Skulan, Henry Sun, Sue Welch, Rene Wiesli, and Kosei Yamaguchi have added greatly to our understanding of Fe isotope geochemistry in experimental and natural systems.

REFERENCES

Aisen P (1994) Iron metabolism: an evolutionary perspective. *In*: Iron Metabolism in Health and Disease. Brock JH, Halliday JW, Pippard MJ, Powell LW (eds) WB Saunders, London, p 1-30

Anbar AD, Roe JE, Barling J, Nealson KH (2000) Nonbiological fractionation of iron isotopes. Science 288: 126-128

Anbar AD, Jarzecki AA, Spiro TG (2004) Theoretical investigation of iron isotope fractionation between $Fe(H_2O)_6^{3+}$ and $Fe(H_2O)_6^{2+}$: implications for iron stable isotope geochemistry. Geochim Cosmochim Acta, in press

Appelo CAJ, VanDerWeiden MJJ, Tournassat C, Charlet L (2002) Surface complexation of ferrous iron and carbonate on ferrihydrite and the mobilization of arsenic. Environ Sci Techno 36:3096-3103

Ardizzone S, Formaro L (1983) Temperature induced phase transformation of metastable $Fe(OH)_3$ in the presence of ferrous ions. Mat Chem Phys 8:125-133

Baker JC, Kassan J, Hamilton PJ (1995) Early diagenetic siderite as an indicator of depositional environment in the Triassic Rewan Group, southern Bowen Basin, eastern Australia. Sedimentology 43:77-88

Barghoorn ES (1981) Aspects of Precambrian paleobiology: the early Precambrian. Paleobot Paleoecol Evolution 1:1-16

Bau M, Dulski P (1996) Distribution of yttrium and rare-earth elements in the Penge and Kuruman iron-formations, Transvaal Supergroup, South Africa. Precam Res 79:37-55

Bau M, Hohndorf A, Dulski P, Beukes NJ (1997) Sources of rare-earth elements and iron in Paleoproterozoic iron-formations from the Transvaal Supergroup, South Africa: evidence from neodymium isotopes. J Geol 105:121-129

Baur ME, Hayes JM, Studley SA, Walter MR (1985) Millimeter-scale variations of stable isotope abundances in carbonates from banded iron-formations in the Hamersley Group of Western Australia. Econ Geol 80: 270-282

Beard BL, Johnson CM (1999) High precision iron isotope measurements of terrestrial and lunar materials. Geochim Cosmochim Acta 63:1653-1660

Beard BL, Johnson CM (2004) Fe isotope variations in the modern and ancient earth and other planetary bodies. Rev Mineral Geochem 55:319-357

Beard BL, Johnson CM, Cox L, Sun H, Nealson KH, Aguilar C (1999) Iron isotope biosignatures. Science 285:1889-1892

Beard BL, Johnson CM, Skulan JL, Nealson KH, Cox L, Sun H (2003a) Application of Fe isotopes to tracing the geochemical and biological cycling of Fe. Chem Geol 195:87-117

Beard BL, Johnson CM, Von Damm KL, Poulson RL (2003b) Iron isotope constraints on Fe cycling and mass balance in oxygenated Earth oceans. Geology 31:629-632

Beliaev AS, Saffarini DA, McLaughlin JL, Hunicutt D (2001) MtrC, an outer membrane decahaem *c* cytochrome required for metal reduction in *Shewanella putrefaciens* MR-1. Mol Microbio 39:722-730

Benz M, Brune A, Schink B (1998) Anaerobic and aerobic oxidation of ferrous iron neutral pH by chemoheterotrophic nitrate-reducing bacteria. Arch Microbiol 169:159-165

Beukes NJ, Klein C (1990) Geochemistry and sedimentology of a facies transition - from microbanded to granular iron-formation - in the early Proterozoic Transvaal Supergroup, South Africa. Precam Res 47: 99-139

Beukes NJ, Klein C, Kaufman AJ, Hayes JM (1990) Carbonate petrography, kerogen distribution, and carbon and oxygen isotope variations in an Early Proterozoic transition from limestone to iron-formation deposition, Transvaal Supergroup, South Africa. Econ Geol 85:663-690

Brantley SL, Liermann L, Bullen TD (2001) Fractionation of Fe isotopes by soil microbes and organic acids. Geology 29:535-538

Brantley SL, Liermann LJ, Guynn RL, Anbar A, Icopini GA, Barling J (2004) Fe isotopic fractionation during mineral dissolution with and without bacteria. Geochim Cosmochim Acta, in press

Brasier MD, Green OR, Jephcoat AP, Kleppe AK, Van Kranendonk MJ, Lindsay JF, Steele A, Grassineau NV (2002) Questioning the evidence for Earth's oldest fossils. Nature 416:76-81

Braterman PS, Cairns-Smith AG (1987) Photoprecipitation and the banded iron-formations. In: The Precambrian Iron-Formations. Appel PWU, LaBerge GL (eds) Theophrastus Pub, Athens, p 215-245

Brown DA, Gross GA, Sawicki JA (1995) A review of the microbial geochemistry of banded iron-formations. Canad Mineral 33:1321-1333

Bullen TD, White AF, Childs CW, Vivit DV, Schultz MS (2001) Demonstration of significant abiotic iron isotope fractionation in nature. Geology 29:699-702

Burgos WD, Royer RA, Fang Y, Yeh GT, Fisher AS, Jeon BH, Dempsey BA (2002) Theoretical and experimental considerations related to reaction-based modeling: a case study using Iron(III) oxide bioreduction. Geomicro J 19:253-287

Butler P (1969) Mineral compositions and equilibria in the metamorphosed iron-formation of the Gagnon region, Quebec, Canada. J Petrol 10:56-101

Caccavo F, Das A (2002) Adhesion of dissimilatory Fe(III)-reducing bacteria to Fe(III) minerals. Geomicro J 19:161-177

Caccavo F, Lonergan DJ, Lovley DR, Davis M, Stolz JF, McInerney MJ (1994) *Geobacter sulfurreducens sp. nov.*, a hydrogen- and acetate-oxidizing dissimilatory metal-reducing microorganism. App Environ Microbio 60:3752-3759

Caccavo F, Schamberger PC, Keiding K, Nielsen PH (1997) Role of hydrophobicity in adhesion of the dissimilatory Fe(III)-reducing bacterium *Shewanella alga* to amorphous Fe(III) oxide. App Environ Microbio 63:3837-3843

Canfield DE, Raiswell R, Bottrell S (1992) The reactivity of sedimentary iron minerals toward sulfide. Am J Sci 292:659-683

Canfield DE, Jørgensen BB, Fossing H, Glud R, Gundersen J, Ramsing NB, Thamdrup B, Hansen JW, Nielsen LP, Hall POJ (1993) Pathways of organic carbon dioxide oxidation in three continental margin sediments. Marine Geol 113:27-40

Chang SBR, Kirschvink JL (1985) Possible biogenic magnetite fossils from the Late Miocene Potamida clays of Crete. *In*: Magnetite Biomineralization and Magnetoreception in Organisms. Kirschvink JL, Jones DS, MacFadden BJ (eds) Plenum Press, New York, p 647-669

Chang SBR, Stolz JF, Kirschvink JL, Awramik SM (1989) Biogenic magnetite in stromatolites II. Occurrences in ancient sedimentary environments. Precam Res 43:305-315

Cloud PE (1965) Significance of the Gunflint (Precambrian) microflora. Science 148:27-45

Cloud P (1968) Atmospheric and hydrospheric evolution on the primitive earth. Science 160:729-736

Coleman ML (1993) Microbial processes - controls on the shape and composition of carbonate concretions. Marine Geol 113:127-140

Coleman ML, Hedrick DB, Lovely DR, White DC, Pye K (1993) Reduction of Fe(III) in sediments by sulphate-reducing bacteria. Nature 361:436-438

Cornell RM, Schwertmann U (1996) The iron oxides: structure, properties, reaction, occurrence and uses. VCH, Weinheim, Germany

Croal LR, Johnson CM, Beard BL, Newman DK (2004) Iron isotope fractionation by anoxygenic Fe(II)-phototrophic bacteria. Geochim Cosmochim Acta 68:1227-1242

Curtis CD, Coleman ML, Love LG (1986) Pore water evolution during sediment burial from isotopic and mineral chemistry of calcite, dolomite and siderite concretions. Geochim Cosmochim Acta 50:2321-2334

DePaolo DJ (1981) Trace element and isotopic effects of combined wallrock assimilation and fractional crystallization. Earth Planet Sci Lett 53:189-201

DiChristina TJ, Moore CM, Haller CA (2002) Dissimilatory Fe(III) and Mn(IV) reduction by *Shewanella putrefaciens* requires *ferE*, a homolog of the *pulE* (*gspE*) Type II protein secretion gene. J Bacteriol 185: 142-151

Dubiel M, Hsu CH, Chien CC, Mansfeld F, Newman DK (2002) Microbial iron respiration can protect steel from corrosion. App Environ Microbio 68:1440-1445

Dzombak DA, Morel FMM (1990) Surface Complexation Modeling: Hydrous Ferric Oxide. John Wiley and Sons

Eggar-Gibbs ZG, Jude B, Dominik J, Loizeau JL, Oldfield F (1999) Possible evidence for dissimilatory bacterial magnetite dominating the magnetic properties of recent lake sediments. Earth Planet Sci Lett 168:1-6

Ehrenreich A, Widdel F (1994) Anaerobic oxidation of ferrous iron by purple bacteria, a new type of phototrophic metabolism. App Environ Microbio 60:4517-4526

Ehrlich HL (1996) Geomicrobiology. 3rd Edn. Marcel Dekker, New York, NY

Eiler JM, Mojzsis SJ, Arrhenius G (1997) Carbon isotope evidence for early life; discussion. Nature 386:665

Emerson D (2000) Microbial oxidation of Fe(II) and Mn(II) at circumneutral pH. *In*: Environmental metal-microbe interactions. Lovley DR (ed) ASM Press, Washington DC, p 31-52

Ewers WE (1983) Chemical factors in the deposition and diagenesis of banded iron-formation. *In*: Iron formations: facts and problems. Trendall AF, Morris RC (eds) Elsevier, Amsterdam, p 491-512

Farley KJ, Dzombak DA, Morel FMM (1985) A surface precipitation model for the sorption of cations on metal oxides. J Colloid Interface Sci 106:226-242

Fedo CM, Whitehouse MJ (2002) Metasomatic origin of quartz-pyroxene rock, Akilia, Greenland, and implications for Earth's earliest life. Science 296:1448-1452

Floran RJ, Papike JJ (1975) Petrology of the low-grade rocks of the Gunflint Iron Formation, Ontario-Minnesota. Geol Soc Amer Bull 86:1169-1190

Frankel RB, Blakemore RP, Wolfe RS (1979) Magnetite in freshwater magnetotactic bacteria. Science 203: 1355-1356

Frankel RB, Blakemore RP, Torres de Araujo FF, Esquivel DMS, Danon J (1981) Magnetotactic bacteria at the geomagnetic equator. Science 212:1269-1270

Fredrickson JK, Zachara JM, Kennedy DW, Dong H, Onstott TC, Hinman NW, Li S (1998) Biogenic iron mineralization accompanying the dissimilatory reduction of hydrous ferric oxide by a groundwater bacterium. Geochim Cosmochim Acta 62:3239-3257

Gaspard S, Vazques F, Holliger C (1998) Localization and solubilization of the Fe(II) reductase of *Geobacter sulfurreducens*. App Environ Microbio 64:3188-3194

Ghiorse WC (1989) Manganese and iron as physiological electron donors and acceptors in aerobic-anaerobic transition zones. *In:* Microbial mats. Cohen Y, Rosenberg E (eds) ASM Press, Washington DC, p 163-179

Glasauer S, Langley S, Beveridge TJ (2002) Intracellular iron minerals in a dissimilatory iron-reducing bacterium. Science 295:117-119

Glasauer S, Weidler PG, Langley S, Beveridge TJ (2003) Controls on Fe reduction and mineral formation by a subsurface bacterium. Geochim Cosmochim Acta 67:1277-1288

Haderlein SB, Pecher K (1999) Pollutant reduction in heterogeneous Fe(II)-Fe(III) systems. *In*: Mineral-water interfacial reactions. Sparks DL, Grundl TJ (eds) American Chemical Society, Washington, DC, p 342-347

Hansel CM, Benner SG, Neiss J, Dohnalkova A, Kukkadapu RK, Fendorf S (2003) Secondary mineralization pathways induced by dissimilatory iron reduction of ferrihydrite under advective flow. Geochim Cosmochim Acta 67:2977-2992

Harder EC (1919) Iron-depositing bacteria and their geologic relations. US Geol Surv Prof Pap 113

Hartman H (1984) The evolution of photosynthesis and microbial mats: a speculation on banded iron formations. *In:* Microbial Mats: Stromatolites. Cohen Y, Castenholz RW, Halvorson HO (eds) Alan Liss Pub, New York, p 451–453

Heising S, Schink B (1998) Phototrophic oxidation of ferrous iron by *Rhodomicrobium vanniellii* strain. Microbiology 144:2263-2269

Heising S, Richter L, Ludwig W, Schink B (1999) *Chlorobium ferrooxidans sp. nov.*, a phototrophic green sulfur bacterium that oxidizes ferrous iron in coculture with a *"Geospirillum" sp.* strain. Arch Microbiol 172:116-124

Hendry JP (2002) Geochemical trends and paleohydrological significance of shallow burial calcite and ankerite cements in Middle Jurassic strata on the East Midlands Shelf (onshore UK). Sed Geol 151:149-176

Hering JG, Stumm W (1990) Oxidative and reductive dissolution of minerals. Rev Mineral 23:427-465

Hernandez ME, Newman DK (2001) Review: Extracellular electron transfer. Cell Mol Life Sci 58:1562-1571

Hernandez ME, Kappler A, Newman DK (2004) Phenazines and other redox-active antibiotics promote microbial mineral reduction. App Environ Microbio 70:921-928

Holland HD (1984) The Chemical Evolution of the Atmosphere and Oceans. Princeton Univ Press, Princeton

Icopini GA, Anbar AD, Ruebush SS, Tien M, Brantley SL (2004) Iron isotope fractionation during microbial reduction of iron: the importance of adsorption. Geology 32:205-208

Jeschke AA, Dreybrodt W (2002) Dissolution rates of minerals and their relation to surface morphology. Geochim Cosmochim Acta 66:3055-3062

Johnson CM, Skulan JL, Beard BL, Sun H, Nealson KH, Braterman PS (2002) Isotopic fractionation between Fe(III) and Fe(II) in aqueous solutions. Earth Planet Sci Lett 195:141-153

Johnson CM, Beard BL, Beukes NJ, Klein C, O'Leary JM (2003) Ancient geochemical cycling in the Earth as inferred from Fe isotope studies of banded iron formations from the Transvaal Craton. Contrib Mineral Petrol 144:523-547

Johnson CM, Roden EE, Welch SA, Beard BL (2004a) Experimental constraints on Fe isotope fractionation during magnetite and Fe carbonate formation coupled to dissimilatory hydrous ferric oxide reduction. Geochim Cosmochim Acta, in press

Johnson CM, Beard BL, Albarède F (2004b) Overview and general concepts. Rev Mineral Geochem 55:1-24

Kalinowski BE, Liermann LJ, Brantley SL, Barnes A, Pantano CG (2000) X-ray photoelectron evidence for bacteria-enhanced dissolution of hornblende. Geochim Cosmochim Acta 64:1331–1343

Kappler A, Newman DK (2004) Formation of Iron(III)-minerals by Iron(II)-oxidizing photoautotrophic bacteria. Geochim Cosmochim Acta 68:1217-1226

Karlin R, Lyle M, Heath CR (1987) Authigenic magnetite formation in suboxic marine sediments. Nature 326: 490-493

Kaufman AJ (1996) Geochemical and mineralogic effects of contact metamorphism on banded iron-formation: an example from the Transvaal Basin, South Africa. Precam Res 79:171-194

Kim J, Dong H, Seabaugh J, Newell SW, Eberl DD (2004) Role of microbes in the smectite-to-illite reaction. Science 203:830-832

Klein C (1974) Greenalite, stilpnomelane, minnesotaite, crocidolite, and carbonates in a very low-grade metamorphic Precambrian iron-formation. Can Min 12:475-498

Klein C (1978) Regional metamorphism of Proterozoic iron-formation, Labrador Trough, Canada. Am Min 63:898-912

Klein C, Gole MJ (1981) Mineralogy and petrology of parts of the Marra Mamba Iron Formation, Hamersley Basin, western Australia. Am Min 66:507-525

Klein C, Beukes NJ (1989) Geochemistry and sedimentology of a facies transition from limestone to iron-formation deposition in the early Proterozoic Transvaal Supergroup, South Africa. Econ Geol 84:1733-1774

Konhauser K (1998) Diversity of bacterial iron mineralization. Earth Sci Rev 43:91-121

Konhauser KO, Hamade T, Raiswell R, Morrice RC, Ferris FG, Southam G, Canfield DE (2002) Could bacteria have formed the Precambrian banded iron formations? Geology 30:1079-1082

Kostka JE, Stucki JW, Nealson KH, Wu J (1996) Reduction of structural Fe(III) in smectite by a pure culture of *Shewanella putrefaciens* strain MR-1. Clays Clay Min 44:522-529

Kostka JE, Haefele E, Viehweger R, Stucki JW (1999a) Respiration and dissolution of Iron(III)-containing clay minerals by bacteria. Environ Sci Tech 33:3127-3133

Kostka JE, Wu J, Nealson KH, Stucki JW (1999b) The impact of structural Fe(III) reduction by bacteria on the surface chemistry of smectite clay minerals. Geochem Cosmochim Acta 63:3705-3713

Kostka JE, Dalton DD, Skelton H, Dollhopf S, Stucki JW (2002) Growth of Iron(III)-reducing bacteria on clay minerals as the sole electron acceptor and comparison of growth yields on a variety of oxidized iron forms. App Environ Microbio 68:6256-6262

LaBerge GL, Robbins EI, Han TM (1987) A model for the biological precipitation of Precambrian iron-formations geological evidence. In: The Precambrian Iron-Formations. Appel PWU, LaBerge GL (eds) Theophrastus Pub, Athens, p 69-96

Larson O, Postma D (2001) Kinetics of reductive bulk dissolution of lepidocrocite, ferrihydrite, and goethite. Geochim Cosmochim Acta 65:1367-1379

Lasaga AC (1981) Rate laws of chemical reactions. Rev Mineral 8:1-68

Laverne C (1993) Occurrence of siderite and ankerite in young basalts from the Galápagos Spreading Center (DSDP Holes 506G and 507B). Chem Geol 106:27-46

Lesher CM (1978) Mineralogy and petrology of the Sokoman Iron Formation near Ardua Lake, Quebec. Can J Earth Sci 15:480-500

Liermann LJ, Kalinowski BE, Brantley SL, Ferry JG (2000) Role of bacterial siderophores in dissolution of hornblende. Geochim Cosmochim Acta 64:587–602

Liu C, Zachara JM, Gorby YA, Szecsody JE, Brown CF (2001) Microbial reduction of Fe(III) and sorption/precipitation of Fe(II) on *Shewanella putrefaciens* strain CN32. Environ Sci Techn 35:1385-1393

Lloyd JR, Blunt-Harris EL, Lovley DR (1999) The periplasmic 9.6 Kilodalton *c*-type cytochrome of *Geobacter sulfurreducens* is not an electron shuttle to Fe(III). J Bact 181:7647-7649

Lloyd JR, Sole VA, van Praagh CVG, Lovley DR (2000) Direct and Fe(II)-mediated reduction of technetium by Fe(III)-reducing bacteria. App Environ Microbio 66:3743-3749

Lovley DR (1987) Organic matter mineralization with the reduction of ferric iron: a review. Geomicro J 5: 375-399

Lovley DR (1991) Dissimilatory Fe and Mn reduction. Microbio Rev 55:259-287

Lovley DR, Phillips EJP (1988) Novel mode of microbial energy metabolism: organic carbon oxidation coupled to dissimilatory reduction of iron or manganese. App Environ Microbio 54:1472-1480

Lovley DR, Stolz JF, Nord Jr GL, Phillips EJP (1987) Anaerobic production of magnetite by a dissimilatory iron-reducing microorganism. Nature 330:252-254

Lovley DR, Coates JD, Blunt-Harris EL, Phillips EJP, Woodward JC (1996) Humic substances as electron acceptors for microbial respiration. Nature 382:445-448

Lowenstam HA (1981) Minerals formed by organisms. Science 211:1126-1131

Machamer JF (1968) Geology and origin of the iron ore deposits of the Zenith mine, Vermilion district, Minnesota. Minn Geol Surv Spec Pub Series 2:1-56

Macquaker JHS, Curtis CD, Coleman ML (1997) The role of iron in mudstone diagenesis: Comparison of Kimmeridge Clay Formation mudstones from onshore and offshore (UKCS) localities. J Sed Res 67: 871-878

Magnuson TS, Hodges-Myerson AL, Lovley DR (2000) Characterization of a membrane-bound NADH-dependent Fe^{3+} reductase from the dissimilatory Fe^{3+}-reducing bacterium *Geobacter sulfurreducens*. FEMS Microbio Lett 185:205-211

Mandal LN (1961) Transformation of iron and manganese in water-logged rice soils. Soil Sci 121-126

Mandernack KW, Bazylinski DA, Shanks III WC, Bullen TD (1999) Oxygen and iron isotope studies of magnetite produced by magnetotactic bacteria. Science 285:1892-189

Mann S, Sparks NHC, Couling SB, Larcombe MC, Franke RB (1989) Crystallochemical characterization of magnetite spinels prepared from aqueous solution. J Chem Soc Far Trans 85:3033-3044

Matthews A, Zhu XK, O'Nions K (2001) Kinetic iron stable isotope fractionation between iron (-II) and (-III) complexes in solution. Earth Planet Sci Lett 192:81-92

Matthews A, Morgans-Bell HS, Emmanuel S, Jenkyns HC, Erel Y, Halicz L (2004) Controls on iron-isotope fractionation in organic-rich sediments (Kimmeridge Clay, Upper Jurassic, southern England). Geochem Cosmochim Acta, in press

Mojzsis SJ, Arrhenius G, McKeegan KD, Harrison TM, Nutman AP, Friend CRL (1996) Evidence for life on Earth before 3,800 million years ago. Nature 384:55-59

Mozely PS (1989) Relationship between depositional environment and the elemental composition of early diagenetic siderite. Geology 17:704-706

Mozley PS, Carothers WW (1992) Elemental and isotopic compositions of siderite in the Kuparuk formation, Alaska: effect of microbial activity and water/sediment interaction on early pore-water chemistry. J Sed Pet 62:681-692

Mozley PS, Wersin P (1992) Isotopic composition of siderite as an indicator of depositional environment. Geology 20:817-820

Mozley PS, Burns SJ (1993) Oxygen and carbon isotopic composition of marine carbonate concretions: an overview. J Sed Pet 63:73-83

Myers CR, Myers JM (1993) Ferric reductase is associated with the membranes of anaerobically grown *Shewanella putrefaciens* MR-1. FEMS Microbio Lett 108:15-22

Myers CR, Nealson KH (1988) Bacterial manganese reduction and growth with manganese oxide as the sole electron acceptor. Science 240:1319-1321

Myers JM, Myers CR (2000) Role of the tetraheme cytochrome *CymA* in anaerobic electron transport in cells of *Shewanella putrefaciens* MR-1 with normal levels of menaquinone. Am Soc Microbio J Bact 183: 67-75

Nealson KH (1983) The microbial iron cycle. *In:* Microbial geochemistry. Krumbein W (ed) Blackwell Sci, Boston, p 159-190

Nealson KH, Myers CR (1990) Iron reduction by bacteria: a potential role in the genesis of banded iron formations. Amer Jour Sci 290A:35-45

Nealson KH, Saffarini D (1994) Iron and manganese in anaerobic respiration: environmental significance, phylogeny, and regulation. Ann Rev Microbio 48:311-343

Nealson KH, Stahl DA (1997) Microorganisms and biogeochemical cycles: what can we learn from layered microbial communities? Rev Mineral 35:5-34

Nevin KP, Lovley DR (2000) Lack of production of electron-shuttling compounds or solubilization of Fe(III) during reduction of insoluble Fe(III) oxide by *Geobacter metallireducens*. App Environ Microbio 66: 2248-2251

Nevin KP, Lovley DR (2002a) Mechanisms for Fe(III) oxide reduction in sedimentary environments. Geomicrobio J 19:141-159

Nevin KP, Lovley DR (2002b) Mechanisms for accessing insoluble Fe(III) oxide during dissimilatory Fe(III) reduction by *Geothrix fermentans*. App Environ Microbio 68:2294-2299

Newman DK, Kolter R (2000) A role for excreted quinones in extracellular electron transfer. Nature 405: 94-97

Nicholson AM, Stolz JF, Pierson BK (1987) Structure of a microbial mat at Great Sippewissett Marsh, Cape Cod, Massachusetts. FEMS Microb Ecol 45:343-363

Parmar N, Warren LA, Roden EE, Ferris FG (2000) Solid phase capture of strontium by the iron reducing bacteria *Shewanella alga* strain BrY. Chem Geol 169:281-288

Pearson MJ (1974) Sideritic concretions from the Westphalian of Yorkshire: a chemical investigation of the carbonate phase. Min Mag 39:696-699

Pierson BK, Parenteau MN (2000) Phototrophs in high iron microbial mats: microstructure of mats in iron-depositing hot springs. FEMS Microb Ecol 32:181-196

Pierson BK, Parenteau MN, Griffin BM (1999) Phototrophs in high-iron concentration microbial mats: physiological ecology of phototrophs in an iron-depositing hot spring. App Environ Microbio 65: 5474-5483

Polyakov VB, Mineev SD (2000) The use of Mössbauer spectroscopy in stable isotope geochemistry. Geochim Cosmochim Acta 64:849-865

Postma D (1977) The occurrence and chemical composition of recent Fe-rich mixed carbonates in a river bog. J Sed Pet 47:1089-1098

Postma D (1981) Formation of siderite and vivianite and the pore-water composition of a recent bog sediment in Denmark. Chem Geol 31:225-244

Postma D (1982) Pyrite and siderite formation in brackish and freshwater swamp sediments. Amer J Sci 282: 1151-1183

Poulson RL, Beard BL, Johnson CM (2003) Investigating isotope exchange between dissolved aqueous and precipitated amorphous iron species in natural and synthetic systems. 13th Ann Goldschmidt Meeting, abstract A382

Pye K, Dickson JAD, Schiavon N, Coleman ML, Cox M (1990) Formation of siderite-Mg-calcite-iron sulphide concretions in intertidal marsh and sandflat sediments, north Norfolk, England. Sedimentology 37:325-343

Raiswell R, Fisher QJ (2000) Mudrock-hosted carbonate concretions: a review of growth mechanisms and their influence on chemical and isotopic composition. J Geol Soc 157: 239-251

Roden EE, Lovley DR (1993) Dissimilatory Fe (III) reduction by the marine microorganism *Desulfuromonas acetoxidans*. App Environ Microbio 59:734-742

Roden EE, Zachara JM (1996) Microbial reduction of crystalline iron(III) oxides: influence of oxide surface area and potential for cell growth. Environ Sci Technol 30:1618-1628

Roden EE, Urrutia MM (2002) Influence of biogenic Fe(II) on bacterial reduction of crystalline Fe(III) oxides. Geomicrobio J 19:209-251

Roden EE, Leonardo MR, Ferris FG (2002) Immobilization of strontium during iron biomineralization coupled to dissimilatory hydrous ferric oxide reduction. Geochim Cosmochim Acta 66:2823-2839

Roe JE, Anbar AD, Barling J (2003) Nonbiological fractionation of Fe isotopes: evidence of an equilibrium isotope effect. Chem Geol 195: 69-85

Rouxel O, Dobbek N, Ludden J, Fouquet Y (2003) Iron isotope fractionation during oceanic crust alteration. Chem Geol 202:155-182

Rouxel O, Fouquet Y, Ludden JN (2004) Subsurface processes at the Lucky Strike hydrothermal field, Mid-Atlantic Ridge: evidence from sulfur, selenium and iron isotopes. Geochim Cosmochim Acta, in press

Schauble EA, Rossman GR, Taylor HP (2001) Theoretical estimates of equilibrium Fe-isotope fractionations from vibrational spectroscopy. Geochim Cosmochim Acta 65:2487-2497

Schopf JW (1992) Paleobiology of the Archaen. *In*: The Proterozoic Biosphere: A Multidisciplinary Study. Schopf JW, Klein C (eds) p 25-39

Schopf JW (1993) Microfossils of the early Archean Apex Chert: new evidence of the antiquity of life. Science 260:640-646

Schopf JW, Kudryavtsev AB, Agresti DG, Wdowiak TJ, Czaja AD (2002) Laser-Raman imagery of Earth's earliest fossils. Nature 416:73-76

Seeliger S, Corn-Ruwisch R, Schink B (1998) A periplasmic and extracellular c-type cytochrome of Geobacter sulfurreducens acts as a ferric iron reductase and as an electron carrier to other acceptors or to partner bacteria. J Bacteriol 180:3686-3691

Sharma M, Polizzotto M, Anbar AD (2001) Iron isotopes in hot springs along the Juan de Fuca Ridge. Earth Planet Sci Lett 194:39-51

Shyu JBH, Lies DP, Newman DK (2002) Protective role of tolC in efflux of the electron shuttle anthraquinone-2,6-disulfonate. J Bacteriol 184:1806-1810

Skinner HCW (1993) A review of apatites, iron and manganese minerals and their roles as indicators of biological activity in black shales. Precam Res 61:209-229

Skulan JL, Beard BL, Johnson CM (2002) Kinetic and equilibrium Fe isotope fractionation between aqueous Fe(III) and hematite. Geochim Cosmochim Acta 66:2995-3015

Sørensen J, Jeørgensen BB (1987) Early diagenesis in sediments from Danish coastal waters: microbial activity and Mn-Se-S geochemistry. Geochim Cosmochim Acta 51:1583-1590

Stahl LJ, Van Gemerden H, Krumbein WE (1985) Structure and development of a benthic microbial mat. FEMS Microbio Ecol 31:111-125

Straub KL, Benz M, Schink B, Widdel F (1996) Anaerobic, nitrate-dependent microbial oxidation of ferrous iron. App Environ Microbio 62:1458-1460

Straub KL, Benz M, Schink B (2001) Iron metabolism in anoxic environments at near neutral pH. FEMS Microbio Ecol 34:181-186

Sumner DY (1997) Carbonate precipitation and oxygen stratification in Late Archean seawater as deduced from facies and stratigraphy of the Gamohaan and Frisco Formations, Transvaal Supergroup, South Africa. Am J Sci 297:455-487

Thamdrup B, Canfield DE (1996) Pathways of carbon oxidation in continental margin sediments off central Chile. Limnol Oceanogr 41:1629-1650

Thamdrup B, Fossing H, Jeørgensen BB (1994) Manganese, iron and sulfur cycling in a coastal marine sediment, Aarhus Bay, Denmark. Geochim Cosmochim Acta 58:5115-5129

Urrutia MM, Roden EE, Fredrickson JK, Zachara JM (1998) Microbial and geochemical controls on synthetic Fe(III) oxide reduction by *Shewanella alga* strain BrY. Geomicrobio J 15:269-291

Uysal IT, Golding SD, Glikson M (2000) Petrographic and isotope constraints on the origin and evolution of authigenic carbonate minerals and the associated fluid evolution in Late Permian coal measures, Bowen Basin (Queensland), Australia. Sed Geol 136:189-206

Vargas M, Kashefi K, Blunt-Harris EL, Lovley DR (1998) Microbiological evidence for Fe(III) reduction of early Earth. Nature 395:65-67

Wade ML, Agresti DG, Wdowiak TJ, Armendarez LP, Farmer JD (1999) A Mössbauer investigation of iron-rich terrestrial hydrothermal vent systems: lessons for Mars exploration. J Geophys Res 104:8489-8507

Welch SA, Beard BL, Johnson CM, Braterman PS (2003) Kinetic and equilibrium Fe isotope fractionation between aqueous Fe(II) and Fe(III). Geochim Cosmochim Acta 67:4231-4250

Widdel F, Schnell S, Heising S, Ehrenreich A, Assmus B, Schink B (1993) Ferrous iron oxidation by anoxygenic phototrophic bacteria. Nature 362:834-836

Wiesli R, Beard BL, Johnson CM (2004) Experimental determination of Fe isotope fractionation between aqueous Fe(II), siderite and "green rust" in abiotic systems. Chem Geol, submitted

Xiong J, Fischer WM, Inoue K, Nakahara M, Bauer CE (2000) Molecular evidence for the early evolution of photosynthesis. Science 289:1724-1730

Zachara JM, Kukkadapu RK, Fredrickson JK, Gorby YA, Smith SC (2002) Biomineralization of poorly crystalline Fe(III) oxides by dissimilatory metal reducing bacteria (DMRB). Geomicrobio J 19:179-206

Zhu XK, O'Nions RK, Guo YL, Reynolds BC (2000) Secular variation of iron isotopes in North Atlantic deep water. Science 287:2000-2002